SCALING RELATIONS IN DENSITY FUNCTIONAL THEORY AND APPLICATIONS OF ELECTRONIC STRUCTURE METHODS

BY TAKEYCE K. WHITTINGHAM

A dissertation submitted to the

Graduate School—New Brunswick

Rutgers, The State University of New Jersey

in partial fulfillment of the requirements

for the degree of

Doctor of Philosophy

Graduate Program in Chemistry

Written under the direction of

Professors Kieron Burke and Karsten Krogh-Jespersen

and approved by

_____

_____

_____

_____

New Brunswick, New Jersey

May, 2004

ABSTRACT OF THE DISSERTATION

Scaling Relations in Density Functional Theory and Applications of Electronic Structure Methods

by Takeyce K. Whittingham

Dissertation Director: Professors Kieron Burke and Karsten Krogh-Jespersen

Today, Density Functional Theory (DFT) is one of the most widely applied of the electronic structure methods. DFT lends itself to research and application in all of the physical sciences. Known for its rigor, reliability, and efficiency, DFT is the computational method of choice for many problems in quantum chemistry, such as determination of reaction pathways and the kinetics and thermodynamics of reactions. Presently, efforts are being made to apply DFT to systems of biological interest that would otherwise be unfeasible with traditional wavefunction methods. Although much of present research in DFT development focuses on an extension of the theory to treat time-dependence, this dissertation explores the development of fundamental aspects of the ground state theory and applications to systems of chemical, biological, and industrial interest. In particular, we extend the usual scaling relations used in density functional development to the low

and high density limits and to scaling the densities of spin channels separately. We also apply DFT to the study of models for organometallic catalysts used in the dehydrogenation of alkanes to form alkenes and to the study of electronic excitations in a few popular anti-cancer drugs.

Acknowledgements

I thank my advisors, Professors Kieron Burke and Karsten Krogh-Jespersen, for their guidance and support over the years. Thanks also to members of each of their groups, past and present, who have contributed considerably to my learning through numerous useful discussions during the course of my graduate study: Heiko Appel, Margaret Czerw, Maxime Dion, Rene Gaudoin, Paul Hessler, Aiyan Lu, Neepa Maitra, Rudolph Magyar, Eunji Sim, Eugene Tsiper, Adam Wasserman, Jan Werschnik, Federico Zahariev, and Fan Zhang

I am grateful for the support and encouragement of my friends Latoria Banks, Stephanie and Robert Banks, April Chin, Olivia Debrah, Tedra and Alvin Gilmore, Julio and Li da Graca, Neepa Maitra and Chris Woodward, Anna Mathauser, Anik Roy and Michel Robillard, Seema Sharma and Sachin Ganu, Sonia Walton, and Adam Wasserman.

Special thanks to Dean Evelyn Erenrich and Professor Wilma Olson who have mentored me and have been instrumental in advising me regarding career options.

Last, I thank my family for their continued love and emotional and financial support: Mom, Dad, my brothers Mario and Aubreyne, my aunt, Margaret Sinclair, my uncles Fitzgerald, Welsford, Aubrey (and wife Leah Guanzón), and Lancelot Sinclair; without whom my success and completion of graduate studies would not have been possible. Above all, I thank God.

Dedication

I dedicate this dissertation to my parents, Beverly and Rhyne Whittingham, for all their prayers, support, countless sacrifices, and unconditional love over the years.

Table of Contents

List of Tables

List of Figures

List of Abbreviations

ADFT	atomic density functional theory code
BLYP	Becke-Lee-Yang-Parr functional
BO	Born-Oppenheimer
C	correlation
CI	configuration interaction
CPT	s-camptothecin
DF	density functional
DFT	density functional theory
ECP	effective core potential
EXX	exact exchange
GGA	generalized gradient approximation
HF	Hartree-Fock
KS	Kohn-Sham
LDA	local density approximation
LSD	local spin-density
MO	molecular orbital
MTX	methotrexate
PBE	Perdew-Burke-Ernzerhof GGA functional
SC	self-consistent
SE	Schrödinger equation
SQP	square pyramidal
TBP	trigonal bipyramidal
X	exchange
XC	exchange-correlation
ΔSCF	Δ self-consistent field

Chapter 1
Electronic Structure Methods

The power and applicability of computational chemistry is widely appreciated and this is evidenced by the range of problems to which it is currently applied [1]. Specific problems include geometry optimizations, calculation of excitation energies, and reactions on surfaces. Computational studies have complemented experimental studies for many years providing, for example, understanding, predictions, and calculations on systems too expensive or dangerous to study experimentally. The emergence of reliable, accurate methods and considerable computer power has made it possible to study systems of increasing size. Traditionally, computational chemists use high-level wavefunction-based methods to give reasonable descriptions and energetics of various systems. For large systems, it is extremely difficult to perform these accurate calculations because of computational cost. Consequently, there is a high demand for rigorous, but computationally feasible methods that can effectively handle the many-body problem.

A promising and proven method widely used in computational chemistry since the 1990s is density functional theory (DFT) [2, 3]. DFT produces good energetics while scaling favorably with electron number. With the advent of DFT and its implementation in computational chemistry, electronic structure calculations on even larger systems are feasible. In addition, DFT provides a remarkable balance between computational cost and accuracy. DFT is applied in many areas including solid state physics where it was first implemented and used successfully for decades. The impact of DFT was recognized with the award of the 1998 Nobel prize in Chemistry to Walter Kohn for his development of the theory [4] and to

John Pople [5] for his contributions to computational chemistry.

A particularly interesting and useful study that shows DFT's power of predictability is the successful discovery of a new, more efficient catalyst for the industrial production of ammonia [6].

There have been significant developments in the design of accurate functionals since the 1990s, which has led to DFT being at the forefront of more accurate methods being developed today. My research has been motivated largely by the need for more accurate functionals. I shall return to a discussion of functionals in section 1.2. First I will briefly review traditional molecular orbital methods.

1.1 Wavefunction-based Methods

There are a number of molecular orbital (MO) methods that are often used in computational chemistry. I will briefly discuss Configuration Interaction, Møller-Plesset Perturbation, and Coupled Cluster theories, which are applied later in chapters 4 and 5.

Every electronic system can be described by a wavefunction according to the Schrödinger equation (SE):

$$\hat{H}\Psi = E\Psi \tag{1.1}$$

where Ψ is the wavefunction for electrons and nuclei, E is the energy, and $\hat{H}$ is the hamiltonian operator given by

$$H = -\sum_i \frac{\hbar^2}{2m_e}\nabla_i^2 - \sum_A \frac{\hbar^2}{2m_A}\nabla_A^2 - \sum_i \sum_A \frac{e^2 Z_A}{r_{iA}} + \sum_{i<j} \frac{e^2}{r_{ij}} + \sum_{A<B} \frac{e^2 Z_A Z_B}{r_{AB}} \tag{1.2}$$

$\hbar$ is Planck's constant divided by 2π, m_e and m_A are the masses of the electrons and nuclei, respectively. ∇^2 is the Laplacian operator; r_{ab} is the inter-particle separation of particles a and b; i, j run over electrons, and A, B run over the nuclei. The wavefunction, Ψ, is then a function of $3N$ coordinates, where N is the total number of particles, electrons and nuclei. Unless otherwise stated, we

shall henceforth use atomic units ($\hbar = e^2 = m_e = 1$), so that all energies are in Hartrees and all lengths in Bohr radii.

As is evident, the motions of the particles are coupled and none moves independently of the other. This presents a very complicated problem, making it impossible to solve exactly. For most systems, the problem can be simplified somewhat by making the Born-Oppenheimer (BO) approximation. Since the nuclei move on a much longer time scale than the electrons, one can ignore the kinetic energy of the nuclei when solving for the electrons, and treat an electronic hamiltonian (the inter-nuclear repulsion also becomes a constant) for each point on a potential energy surface [7].

Even within the BO approximation, it is a daunting task to solve the electronic problem exactly for systems with more than a few electrons. Approximations must be made to the wavefunction.

Hartree developed a self-consistent field (SCF) method wherein one makes an initial guess of the wavefunctions of all occupied atomic orbitals (AOs) in a system [8]. These are then used to construct one electron hamiltonian operators which consist of the kinetic energy of the electrons, the electron-nuclear attraction potential, and an effective potential that approximates the electron-electron repulsion (the Hartree potential). Solving the SE with these one-electron hamiltonians then provides an updated set of wavefunctions and the procedure is repeated until there are no further changes in the updated wavefunctions up to a chosen convergence. This method was extended to molecular systems by Roothaan.[9]

The Pauli exclusion principle states that the electronic wavefunction must be antisymmetric under exchange of any two particles in the system.[10] One clever and simple way to obtain a wavefunction that obeys this principle is to place single-electron orbitals inside a Slater determinant. Fock later extended Hartree's SCF method to Slater determinants. These so-called Hartree-Fock (HF) MOs are eigenfunctions of the set of one-electron hamiltonians. Although an improvement

over Hartree's method, the HF wavefunction cannot be exact because of its restricted form as a Slater determinant. It contains exchange effects but completely neglects any electron correlation.

A first way to introduce correlation is through a perturbative approach. When one is dealing with a Slater determinant approximation, one may express the total energy of a system as the sum of a kinetic energy of electrons, electron-nuclear and nuclear-nuclear interaction energies, electron-electron repulsion energy, and exchange and correlation energies. Møller-Plesset Perturbation theory is defined by setting the exchange energy equal to the HF exchange energy and evaluating the correlation energy from perturbation theory with the HF hamiltonian as the zeroth order hamiltonian (Eqn. 1.3) [11, 12],

$$H = H^{(0)} + \lambda V \tag{1.3}$$

where $H^{(0)}$ is the HF hamiltonian, λ is a dimensionless parameter that changes in value from 0 to 1 and transforms $H^{(0)}$ into H, and V is a perturbing operator that represents the potential due to electron-electron repulsion not included in the HF potential:

$$V = \sum_{\mu<\nu} \frac{1}{r_{\mu\nu}} - \sum_{\mu} V_{\mu}^{eff,HF} \tag{1.4}$$

The method most frequently applied is perturbation up to second order (MP2). Higher order MP theories are much more costly with very little improvement in accuracy.

A further extension is to consider all excitations from the HF determinant, called full configuration interaction (full CI). A full CI calculation with an infinite basis is an exact solution to the non-relativistic, time- independent Schrödinger equation within the BO approximation. Although no reoptimization of HF orbitals is required, it is still extremely computationally demanding to consider all possible excitations for any reasonably sized system of more than 10 electrons [4]. One often considers a limited number of excitations to simplify the calculation.

Most commonly used is CISD where only the complete set of single and double excitations are considered.

Another popular method is coupled cluster theory [13, 14]. This arises from expressing the full CI wavefunction as

$$\Psi = e^T \Psi_{HF} \tag{1.5}$$

$$T = T_1 + T_2 + ... + T_N \tag{1.6}$$

where T is the cluster operator, N is the number of electrons, and the T_i operators give all possible determinants that have i excitations, e.g.

$$T_2 = \sum_{i<j}^{occ.} \sum_{a<b}^{vir.} t_{ij}^{ab} \Psi_{ij}^{ab} \tag{1.7}$$

where Ψ_{ij}^{ab} is a slater determinant with excitations $ij \rightarrow ab$. There are various levels of this, depending on how many excitations are included. In our application of the coupled cluster method in chapter 4, we consider single and double excitations with triples treated non-iteratively (CCSD(T)).

These correlation MO methods are computationally very costly and scale poorly with system size with the best one scaling as N^4, where N is the number of electrons. In the next section we consider a method that is not only often as accurate and reliable, but moreover is computationally less costly; this is particularly important for systems with large numbers of electrons.

1.2 Density Functional Theory, The Method of Choice

It is clear that the external potential, that describes the interaction of the electrons with the nuclei, determines the electronic properties of a system through the Schrödinger equation. The Hohenberg-Kohn theorem [2] proves that the potential is uniquely determined by the ground state electronic density; thus, either can be used as the defining quantity. This is the foundation of Density Functional

Theory. As the name suggests, DFT is based on the fact that all components of the energy of a system can be exactly expressed as functionals of the electronic density and, as such, rather than having to solve the highly-coupled SE for the many-body wavefunction one needs only to determine the electronic density of the system.

The practical power of DFT lies in the mapping of the interacting system to a fictitious system of non-interacting electrons known as the Kohn-Sham (KS) system. The KS system is defined to have the same ground state electronic density as the true, fully interacting, physical system. The result is a set of single-particle equations which are far simpler to solve than the highly correlated Schrödinger equation.

In DFT, the wavefunction is given by a product of Kohn-Sham single particle orbitals. The electronic Hamiltonian operator still consists of kinetic and potential contributions,

$$\left\{-\frac{1}{2}{\nabla_i}^2 + v_{\mathrm{S}}[n](r)\right\}\phi_i = \epsilon_i\phi_i \tag{1.8}$$

but in DFT the break-down of the potential is different. The Kohn-Sham potential, v_{S}, is composed of a Hartree potential (v_{H}), an external potential (v_{ext}), and all that remains is lumped into what is called the exchange-correlation potential (v_{XC}).

$$v_{\mathrm{S}}(\mathbf{r}) = v_{\mathrm{H}}(\mathbf{r}) + v_{\mathrm{ext}}(\mathbf{r}) + v_{\mathrm{XC}}(\mathbf{r}) \tag{1.9}$$

The Hartree potential is given by

$$v_{\mathrm{H}}(\mathbf{r}) = \frac{1}{2}\int d^3\mathbf{r}' \quad \frac{n(\mathbf{r}')}{|\mathbf{r}-\mathbf{r}'|} \tag{1.10}$$

and describes the electrostatic repulsion of the electrons. The external potential uniquely determines the system and expresses the attraction between the nuclei and the electrons and any external field that may be present. In practice, the exchange-correlation potential, a functional of the ground-state density, must be

approximated. If the exact v_{XC} were known, the KS method would provide the exact properties (energies, etc.) of the interacting system.

The electronic density, $n(\mathbf{r})$, is obtained by summing over the occupied Kohn-Sham orbitals, ϕ_i:

$$n(\mathbf{r}) = \sum_{i=1}^{N} |\phi_i(\mathbf{r})|^2 \tag{1.11}$$

and is, in principle, the exact density of the interacting system.

The total energy of the interacting electronic system is expressed as a sum of functionals of the density (hence the name Density Functional Theory):

$$E[n] = T_{\mathrm{S}}[n] + \int d^3\mathbf{r} \;\; n(\mathbf{r}) v_{\mathrm{ext}}(\mathbf{r}) + U[n] + E_{\mathrm{XC}}[n] \tag{1.12}$$

T_{S} is the kinetic energy of the KS system and differs from the kinetic energy, T, of the real system by the kinetic correlation energy T_{C}:

$$T_{\mathrm{S}} = -\frac{1}{2} \sum_{i=1}^{N} \nabla_i^2 \phi_i(\mathbf{r}) \tag{1.13}$$

The hartree energy is given by U:

$$U[n] = \int d^3\mathbf{r} \int d^3\mathbf{r}' \frac{n(\mathbf{r}) n(\mathbf{r}')}{|\mathbf{r} - \mathbf{r}'|} \tag{1.14}$$

The exchange and correlation energies are defined together despite the fact that the exact mathematical representation of the exchange energy is well known in terms of a Fock-like expression. This is because there is a cancellation of errors in approximations to the exchange-correlation term by defining the two together. The exchange-correlation potential is defined as the functional derivative of the exchange correlation energy with respect to the density:

$$v_{\mathrm{XC}}(\mathbf{r}) = \frac{\delta E_{\mathrm{XC}}}{\delta n(\mathbf{r})} \tag{1.15}$$

We note again that the theory is formally exact and would be practically so if the functional dependence of E_{XC} were known. To solve a problem, one need

only approximate the exchange-correlation energy and solve equations 1.8 - 1.11 self consistently. For any given problem, the energy and its components are expressed as functionals of the electronic density. A functional maps a function to a number much like a function maps a number to a number. There are different approximations for the exchange-correlation energy functional, $E_{\mathrm{XC}}[n]$. Typical approximate functionals can be local, semi-local, non-local, or hybrid.

A local density functional depends only on the density at a particular point in space and contains no information about neighboring points. This is the simplest approximation that can be made. An example is the well-known and oft-used local density approximation (LDA [3], also known to users of the popular GAUSSIAN code [15, 16] as SVWN5). This local approximation is exact for a uniform electron gas. The LDA functional works remarkably well despite its simplicity and is extensively used in solid state physics, one of the largest fields where DFT is applied.

Semi-local functionals contain information, not only about the density at a certain point, but also about how the density changes near that point. Semi- and non-local approximations give better descriptions and, consequently, better energies for systems that are more rapidly varying. Generalized Gradient Approximations (GGAs) are semi-local. Examples of popular GGAs in quantum chemistry are the PW91 [17] and PBE [18] functionals which are also often used in solid state physics. Because they are non-empirical, they perform reliably and robustly for a wide variety of systems.

Hybrid functionals represent the exchange energy by a mix of DFT and exact exchange (Hartree Fock exchange). These are often empirical, but not always so [19]. The very popular B3LYP functional [20, 21] which works well for chemical systems is one such example.

1.3 Formal Properties of Exact Functionals: Scaling

With the need for more accurate functional approximations to the exchange-correlation energy, there is great interest in conditions that should be satisfied. If functionals are designed to satisfy some exact conditions, then they will perform better for a large range of problems. One method of testing the accuracy of approximate functionals is to study their behavior under uniform scaling of the electronic density. This method is central to the developmental projects discussed in this thesis.

A scale factor, γ, is introduced which changes the length scale of the density while maintaining normalization. Physically, this either stretches out ($\gamma < 1$) or squeezes up ($\gamma > 1$) the density. The density scales according to

$$n_\gamma(\mathbf{r}) = \gamma^3 n(\gamma \mathbf{r}) \tag{1.16}$$

The prefactor is defined to maintain normalization.

$$N = \int d^3\mathbf{r} \;\; n(\mathbf{r}) = \int d^3\mathbf{r} \;\; \gamma^3 n(\gamma\mathbf{r}) = \int d^3\mathbf{r}' \;\; n(\mathbf{r}') \tag{1.17}$$

Figure 1.3 is a 1d cartoon of the H atom showing the original density, $n(x)$, and the density scaled by $\gamma = 2$ and by $\gamma = 0.5$, $n_{1.5}(x)$.

Performance of approximate functionals can then be tested for their ability to reproduce exact scaling relations. It is straightforward to show that

$$T_\mathrm{s}[n_\gamma] = \gamma^2 T_\mathrm{s}[n] \tag{1.18}$$

$$E_\mathrm{x}[n_\gamma] = \gamma E_\mathrm{x}[n] \tag{1.19}$$

$$U[n_\gamma] = \gamma U[n] \tag{1.20}$$

Since the correlation energy functional is approximated, how it scales cannot be determined exactly. It can, however, be constrained with the following

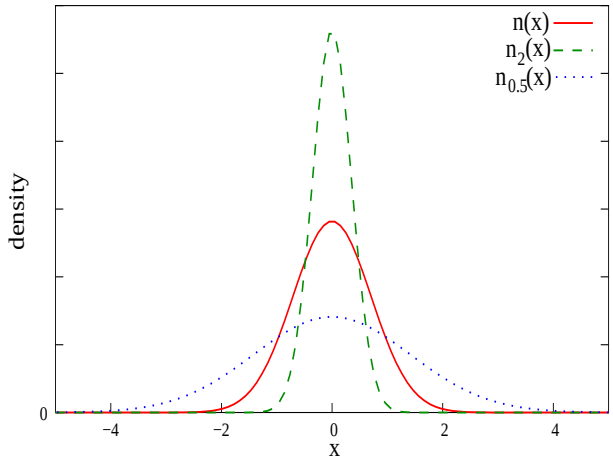

Figure 1.1: Cartoon of the scaled, $n_2(x)$ (dashed line) & $n_{0.5}(x)$ (dotted line), and unscaled, $n(x)$ (solid line), densities of the H atom.

inequality [22]

$$E_{\rm C}[n_\gamma] > \gamma E_{\rm C}[n] \qquad\qquad \gamma > 1 \tag{1.21}$$

One can also derive the virial theorem [23] through scaling relations by noting that small variations in a wavefunction that extremizes the expectation value of the Hamiltonian, $< \hat{H} >$, will give second order changes in the energy. Therefore, a wavefunction scaled by a tiny factor will yield second order changes in $< \hat{H} >$ and its first derivative with respect to γ is zero. Since the Hamiltonian is a sum of kinetic and potential terms, their first derivatives with respect to γ will total zero for some such small variation in the wavefunction. For $\gamma = 1$ in three dimensions we get

$$2T =< \mathbf{r} \cdot \nabla V > \tag{1.22}$$

The virial theorem is satisfied by any eigenstate of the Hamiltonian, so it is a good test of whether or not the problem is solved properly. Evaluating the functionals on scaled densities and seeing how well they reproduce these conditions is one way to test their performance.

Scaling is also related to the adiabatic connection [22] which provides a continuous link between the Kohn-Sham and physical systems. A coupling constant,

λ, which is inversely proportional to γ, is introduced in the Hamiltonian in the following way

$$\hat{H}_\lambda = \hat{T} + \lambda \hat{V}_{\text{ee}} + \hat{V}_{\text{ext}}^\lambda \tag{1.23}$$

The interaction between the electrons in the system is varied while the density remains fixed. $\lambda = 0$ corresponds to the non-interacting Kohn-Sham system and $\lambda = 1$ corresponds to the fully interacting, physical system. The external potential depends implicitly on λ as it must adjust to keep the density fixed.

These are a few manifestations of the importance of scaling in DFT. In chapter 2 we generalize scaling to spin-scaling and show its usefulness for systems with differences in spin densities.

Chapter 2

A New Spin-Decomposition For Density Functionals

The success of GGAs is attributed to their fulfillment of a number of exact conditions. As a result, GGAs are accurate for a range of problems and this fact revolutionized quantum chemistry.

A prominent area of research in DFT is functional development. Of primary importance is understanding functional behavior as a means of improving present approximations. One aspect of my own research has been to work towards defining exact constraints and conditions that functionals should satisfy. Towards that end, we derive exact relations in various limits and test the ability of functionals to reproduce and satisfy these relations.

An accepted methodology for testing approximate functionals in DFT is coordinate scaling. While uniform scaling of the electronic density is a well-studied and fundamental property, scaling the density of each spin channel independently (spin scaling) had not been previously explored.

Proper analysis of spin contributions through spin-decomposition of energies aid in the improvement of DFT treatment of spin polarized systems. By improving spin considerations in present functionals we hope to get better approximations to the exchange-correlation functional. This will increase the accuracy of density functional methods and calculations will become more practical for a number of applications in which spin is important.

We study the performance of existing spin density functionals on a few spin-scaled atoms. This method highlights the limitations of present functional approximations and may be especially important for the treatment of systems for which spin differences are important. These systems include spin-polarized systems such as half-metals, biradicals, and other magnetic systems. This study was completed in collaboration with Rudolph Magyar [25].

2.1 Treatment of spin in DFT

Spin considerations are incorporated into approximate functionals by means of spin DFT [26, 27]. While the total density is the determining factor in any problem, approximate functionals are often more accurate when written in terms of spin densities. The density can be written as a sum of spin densities, $n_\uparrow$ and $n_\downarrow$, where $n_\uparrow$ is the electronic density of up spins only and $n_\downarrow$ is that of the down spins.

$$n(\mathbf{r}) = n_\uparrow(\mathbf{r}) + n_\downarrow(\mathbf{r}) \tag{2.1}$$

It can be shown that the exchange component of the energy can be spin decomposed in the following way

$$E_{\mathrm{X}}[n_\uparrow, n_\downarrow] = \frac{1}{2}(E_{\mathrm{X}}[2n_\uparrow] + E_{\mathrm{X}}[2n_\downarrow]) \tag{2.2}$$

since exchange is only allowed between like spins. This allows for better treatment of magnetized systems and overall more accurate approximations.

The analogous decomposition for correlation is not as simple.

In this chapter, we derive a spin-dependent virial theorem which follows from the spin transformation given above. This has several uses . . . Like the usual virial theorem,[23]

$$\frac{dE_{\mathrm{XC}}[n_\gamma]}{d\gamma} = -\frac{1}{\gamma}\int d^3r n(\mathbf{r})\mathbf{r}\cdot\nabla v_{\mathrm{XC}}[n](\mathbf{r}) \tag{2.3}$$

that can be used to check the convergence of DFT calculations, the spin-dependent virial theorem may be used to check the convergence of spin-density functional calculations. It also provides a method for calculating the exact dependence of the correlation energy on spin-density for model systems for which accurate Kohn-Sham potentials have been found. We use α to denote scaling of one spin density only, in our demonstrations the up spin. Finally, the spin-dependent virial can be integrated over the scale factor α to give a new formal expression for the functional, $E_{\rm XC}$.

Considerable progress has been made in DFT by writing $E_{\rm XC}$ as an integral over the coupling constant λ in the adiabatic connection relationship [28, 29]. The success of hybrid functionals such as B3LYP [20, 21] can be understood in terms of the adiabatic connection [30, 31]. The adiabatic connection is simply related to uniform coordinate scaling [32, 33] as mentioned in chapter 1. Here, in section 2.5, we extend the spin scaling relationship to a spin-coupling constant integration, and define a suitable generalization for this definition of the adiabatic connection with a coupling constant for each spin density.

We use several examples to illustrate our formal results. For the uniform electron gas (section 2.3), we can perform this scaling essentially exactly. We show how this transformation relates energies to changes in spin-polarization. In this case, considerable care must be taken to deal with the extended nature of the system. We also compare popular functional approximations and show their results of spin scaling on the densities of small atoms (section 2.4). Finally, we discuss a fundamental difficulty underlying this spin scaling approach.

Throughout this chapter, we use atomic units ($e^2 = \hbar = m_e = 1$), so that all energies are in Hartrees and all lengths in Bohr radii. We demonstrate all scaling relationships by scaling the up spin densities. Results for scaling the down spin are obtained in a similar fashion.

2.2 Spin scaling theory

We extend total density functional scaling techniques to spin-density functional theory. Scaling each spin's density separately we write

$$\begin{aligned} n_{\uparrow\alpha}(\mathbf{r}) &= \alpha^3 n_\uparrow(\alpha\mathbf{r}), \quad 0 \le \alpha < \infty \\ n_{\downarrow\beta}(\mathbf{r}) &= \beta^3 n_\downarrow(\beta\mathbf{r}), \quad 0 \le \beta < \infty. \end{aligned} \tag{2.4}$$

Accordingly, a spin-unpolarized system becomes spin-polarized when $\alpha \neq \beta$.

The first interesting property of spin scaling is that, although the scaled spin density may tend to zero at any point, the total number of electrons of each spin in the system of interest is conserved during the spin scaling transformation of Eq. (2.4). As the value of α decreases, the two spin densities occupy the same coordinate space, but on two very distinct length scales. Even when $\alpha \to 0$, the up electrons do not vanish, but are merely spread over an infinitely large volume. The scaled density presumably then has a vanishingly small contribution to the correlation energy. For finite systems, we can consider this limit as the effective removal of one spin density to infinitely far way. We will discuss what this means for extended systems later when we treat the uniform gas.

Another interesting property of the spin scaling transformation is that one can express the scaling of one spin density as a total density scaling with one of the spin densities inversely spin scaled.

$$E_{\mathrm{XC}}[n_{\uparrow\alpha}, n_\downarrow] = E_{\mathrm{XC}}[\{\, n_\uparrow, n_{\downarrow 1/\alpha} \,\}_\alpha] \tag{2.5}$$

where the parenthesis notation on the right indicates scaling the total density. Thus, without loss of generality, we need only scale one spin density.

To understand what happens when a single spin density is scaled, we first study exchange. Because the Kohn-Sham orbitals are single particle orbitals, the spin up and down Kohn-Sham orbitals are independent. In addition, exchange occurs only between like-spins. The exchange energy functional can therefore

be split into two parts, one for each spin [24] as in equation 2.2. The scaling relationships for total DFT generalize for each term independently. For an up spin scaling, we spin scale Eq. 2.2 to find

$$\begin{aligned} E_{\rm x}[n_{\uparrow\alpha}, n_\downarrow] &= \frac{1}{2}E_{\rm x}[2n_{\uparrow\alpha}] + \frac{1}{2}E_{\rm x}[2n_\downarrow] \\ &= \frac{\alpha}{2}E_{\rm x}[2n_\uparrow] + \frac{1}{2}E_{\rm x}[2n_\downarrow]. \end{aligned} \tag{2.6}$$

where we have also used exchange energy scaling equation 1.19. When $\alpha \to 0$, we are left with only the down contribution to exchange. Scaling spin densities independently allows us to extract the contribution from each spin channel, e.g., $dE_{\rm x}[n_{\uparrow\alpha}, n_\downarrow]/d\alpha$ at $\alpha = 1$ is the contribution to the exchange energy from the up density. A plot of $E_{\rm x}[n_{\uparrow\alpha}, n_\downarrow]$ versus α between 0 and 1 yields a straight line and is twice as negative at $\alpha = 1$ as at $\alpha = 0$ for an unscaled system that is spin saturated.

Separate spin-scaling of the correlation energy is more complicated. Unlike $E_{\rm x}[n_\uparrow, n_\downarrow]$, it is not trivial to split $E_{\rm C}[n_\uparrow, n_\downarrow]$ into up and down contributions. The Levy method of scaling the exact ground-state wave-function does not yield an inequality such as Eq. (1.21), because the spin-scaled wave-function is not a ground-state of another Coulomb-interacting Hamiltonian. Nor does it yield an equality as in the spin-scaled exchange case, Eq. (2.6), because the many-body wave-function is not simply the product of two single spin wave-functions. In both cases, exchange and correlation, the two spins are coupled by a term $1/|\mathbf{r} - \alpha\mathbf{r}'|$.

To obtain an exact spin scaling relationship for $E_{\rm xc}$, we take a different approach. Consider a change in the energy due a small change in the up-spin density:

$$\delta E_{\rm xc} = E_{\rm xc}[n_\uparrow + \delta n_\uparrow, n_\downarrow] - E_{\rm xc}[n_\uparrow, n_\downarrow]. \tag{2.7}$$

Use $v_{{\rm xc}\uparrow}(\mathbf{r}) = \delta E_{\rm xc}/\delta n_\uparrow(\mathbf{r})$ to rewrite $\delta E_{\rm xc}$ as

$$\delta E_{\rm xc} = \int d^3r \delta n_\uparrow(\mathbf{r})\; v_{{\rm xc}\uparrow}[n_\uparrow, n_\downarrow](\mathbf{r}). \tag{2.8}$$

to first order in $\delta n_\uparrow$. Now, consider this change as coming from the following scaling of the density, $n_{\uparrow\alpha}(\mathbf{r}) = \alpha^3 n_\uparrow(\alpha\mathbf{r})$, where α is arbitrarily close to one. The change in the density is related to the derivative of this scaled density:

$$\frac{dn_{\uparrow\alpha}(\mathbf{r})}{d\alpha}|_{\alpha=1} = 3n_\uparrow(\mathbf{r}) + \mathbf{r}\cdot\nabla n_\uparrow(\mathbf{r}). \tag{2.9}$$

Use Eqs. (2.8) and (2.9), and integrate by parts to find

$$\frac{dE_{\rm XC}[n_{\uparrow\alpha}, n_\downarrow]}{d\alpha}|_{\alpha=1} = -\int d^3r n_\uparrow(\mathbf{r})\ \mathbf{r}\cdot\nabla v_{{\rm XC}\uparrow}[n_\uparrow, n_\downarrow](\mathbf{r}). \tag{2.10}$$

Eq. (2.10) is an exact result showing how $dE_{\rm XC}/d\alpha|_{\alpha=1}$ can be extracted from the spin densities and potentials. For an initially unpolarized system, $n_\uparrow = n_\downarrow = n/2$, and $v_{{\rm XC}\uparrow} = v_{{\rm XC}\downarrow} = v_{\rm XC}$. Thus the right-hand-side of Eq. (2.10) becomes half the usual virial of the exchange-correlation potential (Eq. 2.3). This virial is equal to $dE_{\rm XC}[n_\alpha]/d\alpha|_{\alpha=1} = E_{\rm XC} + T_{\rm C}$.[22] Thus, for spin-unpolarized systems,

$$\frac{dE_{\rm C}[n_{\uparrow\alpha}, n_\downarrow]}{d\alpha}|_{\alpha=1} = \frac{1}{2}\left(E_{\rm C} + T_{\rm C}\right). \tag{2.11}$$

For initially polarized systems, there is no simple relation between the two types of scaling.

To generalize Eq. (2.10) to finite scalings, simply replace $n_\uparrow$ on both sides by $n_{\uparrow\alpha}$, yielding:

$$\frac{dE_{\rm XC}[n_{\uparrow\alpha}, n_\downarrow]}{d\alpha} = -\frac{1}{\alpha}\int d^3r n_{\uparrow\alpha}(\mathbf{r})\ \mathbf{r}\cdot\nabla v_{{\rm XC}\uparrow}[n_{\uparrow\alpha}, n_\downarrow](\mathbf{r}). \tag{2.12}$$

We can then write the original spin-density functional as a scaling integral over this derivative:

$$E_{\rm XC}[n_\uparrow, n_\downarrow] = \lim_{\alpha\to 0} E_{\rm C}[n_{\uparrow\alpha}, n_\downarrow] + \int_0^1 d\alpha \frac{dE_{\rm XC}[n_{\uparrow\alpha}, n_\downarrow]}{d\alpha}. \tag{2.13}$$

This is a new expression for the exchange-correlation energy as an integral over separately spin-scaled densities, where the spin-scaled density is scaled to the low-density limit. With some physically reasonable assumptions, we expect

$$\lim_{\alpha\to 0} E_{\rm C}[n_{\uparrow\alpha}, n_\downarrow] = E_{\rm C}[0, n_\downarrow]. \tag{2.14}$$

For example, if the anti-parallel correlation hole vanishes as rapidly with scale factor as the parallel-spin correlation hole of the scaled density, this result would be true. Numerical results indicate that this is the case for the approximate functionals used in this chapter. Nevertheless, Eq. (2.14) is not proven here.

A symmetric formula can be written down by scaling the up and down spins separately and averaging:

$$\begin{aligned} E_{\rm XC}[n_\uparrow, n_\downarrow] &= \frac{1}{2}\lim_{\alpha\to 0}\left(E_{\rm XC}[n_{\uparrow\alpha}, n_\downarrow] + E_{\rm XC}[n_\uparrow, n_{\downarrow\alpha}]\right) \\ &\quad + \frac{1}{2}\int_0^1 d\alpha \int d^3r n_{\uparrow\alpha}(\mathbf{r})\mathbf{r}\cdot\nabla v_{{\rm XC}\uparrow}[n_{\uparrow\alpha}, n_\downarrow](\mathbf{r}) \\ &\quad + \frac{1}{2}\int_0^1 d\beta \int d^3r n_{\downarrow\beta}(\mathbf{r})\mathbf{r}\cdot\nabla v_{{\rm XC}\downarrow}[n_\uparrow, n_{\downarrow\beta}](\mathbf{r}). \end{aligned} \tag{2.15}$$

This result combines ideas of spin-decomposition, coordinate scaling, and the virial theorem. Each of these ideas yields separate results for pure exchange or uniform coordinate scaling, but all are combined here. Notice that the potentials depend on both spins, one scaled and the other unscaled. This reflects the difficulty in separating up and down spin correlations.

The proof of Eq. (2.15) holds for exchange-correlation, but in taking the weakly-correlated limit, the result also holds true for the exchange limit. In the case of exchange, Eq. (2.15) reduces to Eq. (2.6) with equal contributions from the limit terms and the virial contributions. To obtain this result, recall how $E_{\rm X}$ scales, Eq. (1.19). Since the energy contribution from each spin is separate and since the scaling law is linear, one can take the limits in the first two terms of Eq. (2.15) without making additional physical assumptions. The virial terms are somewhat more difficult to handle as the exchange potentials change under scaling. In the end, one finds that the first two terms contribute half the exchange energy while the virial terms contribute the other half.

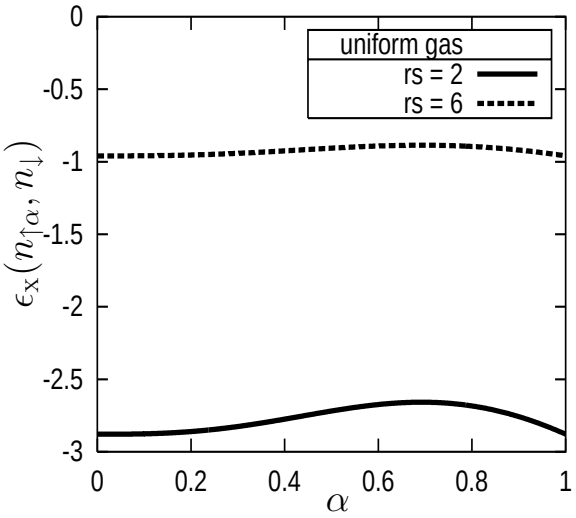

Figure 2.1: Spin scaling of a uniform gas: exchange energy per particle Eq. (2.21), $\epsilon_{\rm x}(n_{\uparrow\alpha}, n_{\downarrow})$, at $r_s = 2$ (dotted line) and 6 (solid line). The spin scaled exchange energy per particle is different than what one might naively expect from Eq. (2.6). This subtlety is discussed in section 2.4.

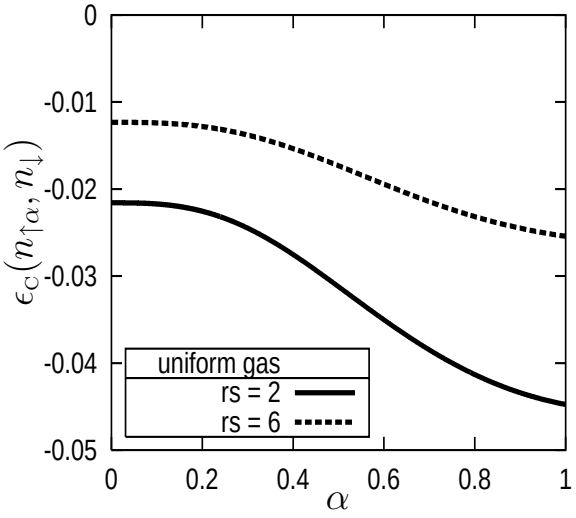

Figure 2.2: Spin scaling of a uniform gas: correlation energy per particle, $\epsilon_{\rm C}(n_{\uparrow\alpha}, n_{\downarrow})$, at $r_s = 2$ (dotted line) and 6 (solid line). The energy per particle is different from what one might naively expect from Eq. (2.6). Section 2.4 discusses this subtlety in detail.

2.3 Uniform gas

We first study the effect of spin scaling on the uniform electron gas as we have essentially numerically exact results. Care is taken when determining quantities for spin scaling in extended systems. We begin with a spin-unpolarized electron gas of density n and Wigner-Seitz radius $r_s = (3/4\pi n)^{\frac{1}{3}}$. When one spin density is scaled, the system becomes spin-polarized, and the relative spin-polarization is measured by

$$\zeta = \frac{n_\uparrow - n_\downarrow}{n_\uparrow + n_\downarrow}. \tag{2.16}$$

We assume that for a spin-polarized uniform system, the exchange-correlation energy per electron, $\epsilon_{\rm XC}^{\rm unif}(r_s, \zeta)$, is known exactly. We use the correlation energy parameterization of Perdew and Wang [17] to make our figures.

To perform separate spin scaling of this system, we focus on a region deep in the interior of any finite but large sample. A simple example is a jellium sphere of radius $R >> r_s$. The correlation energy density deep within will tend to that of the truly translationally invariant uniform gas as $R \to \infty$. At $\alpha = 1$, we have an unpolarized system with $n_\uparrow = n_\downarrow = n/2$. The up-spin scaling, $n_\uparrow = \alpha^3 n/2$, changes both the total density and the spin-polarization. Deep in the interior

$$r_s(\alpha) = r_s \left(\frac{2}{1+\alpha^3} \right)^{1/3} \tag{2.17}$$

where r_s is the Seitz radius of the original unpolarized gas, and

$$\zeta(\alpha) = \frac{\alpha^3 - 1}{\alpha^3 + 1}. \tag{2.18}$$

The exchange-correlation energy density here is then

$$e_{\rm XC}(\alpha) = e_{\rm XC}^{\rm unif}(n_{\uparrow\alpha}, n_\downarrow) = e_{\rm XC}^{\rm unif}(r_s(\alpha), \zeta(\alpha)), \tag{2.19}$$

and the energy per particle is

$$\epsilon_{\rm XC}(\alpha) = e_{\rm XC}(\alpha)/n(\alpha) \tag{2.20}$$

where $n(\alpha)$ is the interior density.

Again, for its simplicity, we first consider the case of exchange. Deep in the interior, we have a uniform gas of spin densities $n_{\uparrow\alpha}$ and $n_{\downarrow}$, and the energy densities of these two are given by Eq. (2.6), since the integrals provide simple volume factors. The Slater factor of $n^{4/3}$ in the exchange density of the uniform gas produces a factor of $(1+\alpha^4)$. When transforming to the energy per electron, there is another factor of $(1+\alpha^3)$ due to the density out front. Thus the exchange energy per electron is

$$\epsilon_{\rm x}(\alpha) = \left(\frac{1+\alpha^4}{1+\alpha^3}\right)\ \epsilon_{\rm x}^{unpol.}(n) \tag{2.21}$$

This variation is shown in Fig. 2.1. This result may appear to disagree with Eq. (2.6), but it is valid deep in the interior only. To recover the total exchange energy, one must include those electrons in a shell between R and R/α with the fully polarized uniform density $\alpha^3 n/2$. The exchange energy integral includes this contribution, and then agrees with Eq. (2.6).

Near $\alpha = 1$, Eq. (2.21) yields $(1+\alpha)\ \epsilon_{\rm x}^{unpol.}/2$, in agreement with a naive application of Eq. (2.6). This is because, in the construction of the total energy from the energy per electron, the factor of the density accounts for changes in the number of electrons to first order. So the derivative at $\alpha = 1$ remains a good measure of the contribution to the total exchange energy from one spin density. On the other hand, as $\alpha \to 0$, the exchange energy per electron in the interior returns to that of the original unpolarized case. This reflects the fact that exchange applies to each spin separately, so that the exchange per electron of the down-spin density is independent of the presence of the up-spin density.

Figure 2.2 shows the uniform electron gas correlation energy per particle scaled from unpolarized ($\alpha = 1$) to fully polarized limits ($\alpha = 0$). Again, the curves become flat as $\alpha \to 0$, because for small α, there is very little contribution from the up-spins. Now, however, there is a dramatic reduction in the correlation energy per particle in going from $\alpha = 1$ to $\alpha = 0$ because of the difference in

correlation between the unpolarized and fully polarized gases. Note that the correlation changes tend to cancel the exchange variations.

2.4 Finite Systems

Next, we examine the behavior of finite systems under separate-spin scaling. We choose the He and Li atoms to demonstrate spin scaling effects on the simplest non-trivial initially unpolarized and spin-polarized cases. For each of these atoms, the Kohn-Sham equations are solved using four different functionals. The resulting self-consistent densities are spin scaled and the energies evaluated on these densities for each functional.

Since these are approximate functionals, neither the densities nor the energies are exact. We are unaware of any system, besides the uniform gas, for which exact spin-scaled plots are easily obtainable. For now, we must compare plots generated from approximate functionals. Even the simple atomic calculations presented here were rather demanding since, especially for very small spin-scaling parameters, integrals containing densities on two extremely distinct length scales are needed.

The He atom (Fig. 2.3) is spin unpolarized at $\alpha = 1$. Scaling either spin density gives the same results. In the fully scaled limit, we expect, as we have argued in section 2.2, that the correlation energy should vanish. This is because the two electrons are now on very different length scales and so do not interact with each other. The LSD curve gives far too much correlation and does not vanish as $\alpha \to 0$. The residual value at $\alpha \to 0$ reflects the self-interaction error in LSD for the remaining (unscaled) one-electron density. The PBE curve, although on the right scale, also has a self-interaction error as $\alpha \to 0$, albeit less than the LSD error. The BLYP functional [34, 35] gets both limits correct by construction. The functional's lack of self-interaction error is because its correlation energy vanishes

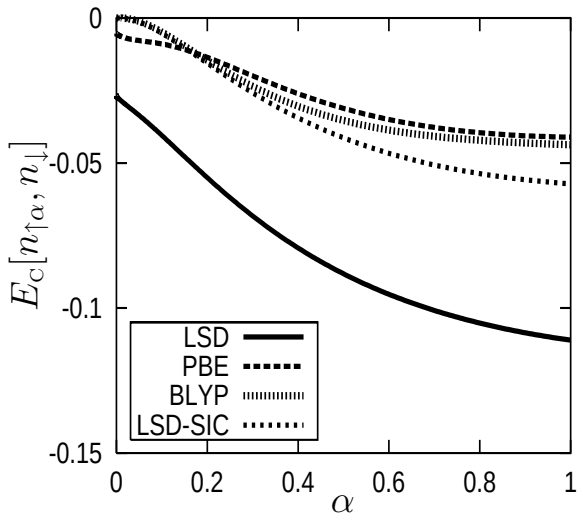

Figure 2.3: Spin scaling of the He atom density using various approximate functionals for $E_{\rm C}$: local spin-density approximation (solid line), generalized gradient approximation (PBE, dashed line), BLYP (bars), and self-interaction corrected LSD (short dashes).

for *any* fully polarized system. This vanishing is incorrect for any atom other than H or He. Finally, the LSD-SIC curve [36] is perhaps the most accurate in shape (if not quantitatively) since this functional handles the self-interaction error appropriately. We further observe that the curves appear quite different from those of the uniform gas. The atomic curves are much flatter near $\alpha \to 1$ and have appreciable slope near $\alpha \to 0$. This is because these energies are integrated over the entire system, including the contribution from the entire spin-scaled density, whereas the energy densities in the uniform gas case were only those in the interior.

Quantitative results are listed in Table 2.1. The exact He values, including the derivative at $\alpha = 1$, using Eq. (2.11), were taken from Ref. [37, 38]. Note that PBE yields the most accurate value for this derivative. The BLYP correlation energy is too flat as function of scale parameter. BLYP produces too small a value for $T_{\rm C}$ leading to a lack of cancellation with $E_{\rm C}$ and a subsequent overestimation of the derivative at $\alpha = 1$. LSD-SIC has a similar problem. The LSD value,

Approx.	$E_{\rm X}$	$E_{\rm C}$	$E_{\rm C}[n_\uparrow, 0]$	$dE_{\rm C}/d\alpha$
LSD	-0.862	-0.111	-0.027	-0.022
PBE	-1.005	-0.041	-0.005	-0.002
SIC	-1.031	-0.058	0.000	-0.011
BLYP	-1.018	-0.044	0.000	-0.005
exact	-1.026	-0.042	0.000	-0.003

Table 2.1: He atom energies, both exactly and within several approximations. All energies in Hartrees; all functionals evaluated on self-consistent densities.

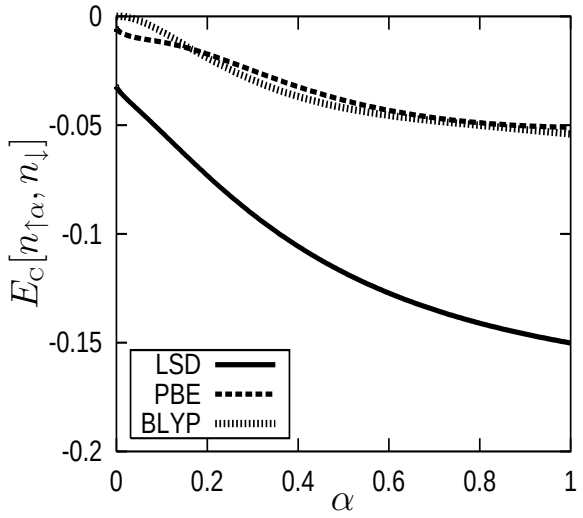

Figure 2.4: Up spin scaling of the Li atom density using various approximate functionals for $E_{\rm C}$: local spin-density approximation (solid line), generalized gradient approximation (PBE, dashed line), and BLYP (bars).

while far too large, is about 8% of the LSD correlation energy, close to the same fraction for PBE, and not far from exact. However, the conclusion here is that results from separate spin-scaling are a new tool for examining the accuracy of the treatment of spin-dependence in approximate spin-density functionals.

The Li atom (Figs.2.4 and 2.5) is the smallest odd many-electron atom. We choose the up spin density to have occupation *1s2s*. As expected, the curve resulting from scaling the up spins away, Fig. 2.4, is very similar to that of He, Fig. 2.3. The primary difference is the greater correlation energy for $\alpha = 1$.

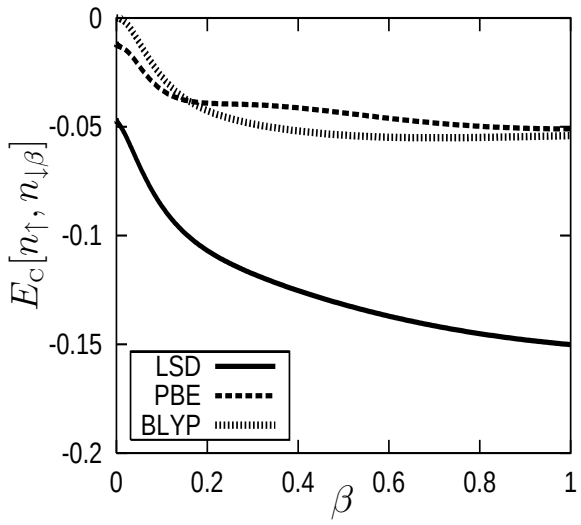

Figure 2.5: Down spin scaling of the Li atom density using various approximate functionals for $E_{\rm C}$: local spin-density approximation (solid line), generalized gradient approximation (PBE, dashed line), and BLYP (bars).

On the other hand, scaling away the down-density gives a very different picture, Fig. 2.5. The most dramatic changes in the correlation energy now occur at small α. Near $\alpha \to 1$, the system energy is quite insensitive to spin-scaling, especially as calculated by the GGAs. This is exactly the opposite of what we have seen in the case of the uniform gas. Whether this would be observed with the exact functional remains unanswered. For up spin scaling, we expect the correlation energy to vanish as $\alpha \to 0$. But for down spin scaling one expects a finite correlation energy in the limit $\beta \to 0$. The two spin-up electrons remain and are still correlated. For the reason stated earlier, the BLYP functional still predicts no correlation energy for the remaining two electrons.

Quantitative results for Li are given in Table 2.2. The exact result for $E_{\rm X}$ is the $E_{\rm X}$ of a self consistent OEP calculation. Using the highly accurate energy prediction from [39], we deduce the exact $E_{\rm C} = E_T - E_{T,OEP}$, where E_T is the exact total energy of the system and $E_{T,OEP}$ is the total energy calculated using DFT exact exchange. The other exact results are not extractable from the literature here, but could be calculated from known exact potentials and densities [40].

Approx.	$E_{\rm X}$	$E_{\rm C}$	$E_{\rm C}[n_\uparrow, 0]$	$dE_{\rm C}/d\alpha$	$E_{\rm C}[0, n_\downarrow]$	$dE_{\rm C}/d\beta$
LSD	-1.514	-0.150	-0.047	-0.037	-0.032	-0.019
PBE	-1.751	-0.051	-0.012	-0.004	-0.005	-0.001
BLYP	-1.771	-0.054	-0.054	-0.020	0.000	-0.005
exact	-1.781	-0.046	-	-	0.000	-

Table 2.2: Li atom energies, both exactly and within several approximations. All energies in Hartrees, all functionals evaluated on self-consistent densities.

Even in this simple case, an SIC calculation is difficult. For the up-spin density, one would need to find the *1s* and *2s* orbitals for each value of α that yield the spin-scaled densities.

2.5 Spin adiabatic connection

Here, we define the adiabatic connection within our spin-scaling formalism. λ is usually a parameter in the Hamiltonian that scales the electron-electron interaction, but this way of thinking becomes prohibitively complicated in spin density functional theory. We would have to define three coupling constants: $\lambda_\uparrow$, $\lambda_\downarrow$, and $\lambda_{\uparrow\downarrow}$. Even so, it remains non-trivial to relate changes in these coupling constants to changes in the electron density. Instead, we define a relationship between spin-scaling and a spin dependent coupling parameter. First, for total density scaling, the relationship between scaling and evaluating a functional at a different coupling constant is [22, 32]

$$E_{\rm XC}^{\lambda}[n] = \lambda^2 E_{\rm XC}[n_{1/\lambda}]. \tag{2.22}$$

where the left hand side means the exchange-correlation energy at an interaction scaled by λ. The adiabatic connection formula is

$$E_{\rm XC} = \int_0^1 d\lambda \, \frac{dE_{\rm XC}^{\lambda}}{d\lambda} = \int_0^1 d\lambda \, U_{\rm XC}(\lambda). \tag{2.23}$$

By virtue of the Hellmann-Feynman theorem [23], $U_{\rm XC}(\lambda)$ can be identified as the potential contribution to exchange-correlation at coupling constant λ. The

integrand $U_{\rm XC}(\lambda)$ can be plotted both exactly and within density functional approximations, and its behavior studied to identify deficiencies of functionals [41]. For separate spin scaling, we apply the same ideas but now to

$$\Delta E_{\rm XC}[n_\uparrow, n_\downarrow] = E_{\rm XC}[n_\uparrow, n_\downarrow] - E_{\rm XC}[0, n_\downarrow], \tag{2.24}$$

that is, the exchange-correlation energy difference between the physical system and the system with one spin density removed while keeping the remaining spin-density fixed. For polarized systems, this quantity depends on which spin density is removed. We now define

$$\Delta E_{\rm XC}^{\lambda_\uparrow} = {\lambda_\uparrow}^2 \Delta E_{\rm XC}[n_{1/\lambda_\uparrow}, n_\downarrow] \tag{2.25}$$

where $\Delta E_{\rm XC}^{\lambda\uparrow}$ is the exchange-correlation energy difference with the interaction of the up spins scaled by $\lambda_\uparrow$, and

$$\Delta U_{\rm XC}(\lambda_\uparrow) = d\Delta E_{\rm XC}^{\lambda_\uparrow}/d\lambda_\uparrow, \tag{2.26}$$

so that

$$\Delta E_{\rm XC} = \int_0^1 d\lambda_\uparrow \; \Delta U_{\rm XC}(\lambda_\uparrow). \tag{2.27}$$

This produces a physically meaningful spin-dependent decomposition of the exchange-correlation energy, with the integral now including the high-density limit. As $\lambda_\uparrow \to 0$, exchange dominates, and $U_{\rm XC}(\lambda_\uparrow) \to U_{\rm X}(\lambda_\uparrow)$ which is just $E_{\rm X}[2n_\uparrow]/2$ according to the simple results for exchange in chapter 1. Furthermore, in the absence of correlation, $U_{\rm XC}(\lambda_\uparrow)$ is independent of $\lambda_\uparrow$. This is not true if one uses a naive generalization of Eq. (2.22).

This spin adiabatic connection formula should prove useful for the improvement of present-day functionals in the same way that the adiabatic connection formula has been useful for improving total density functionals. For example, it may be possible to perform Görling-Levy perturbation theory [42] in this parameter ($\lambda_\uparrow$) or to extract a correlation contribution to kinetic energy [43]. We

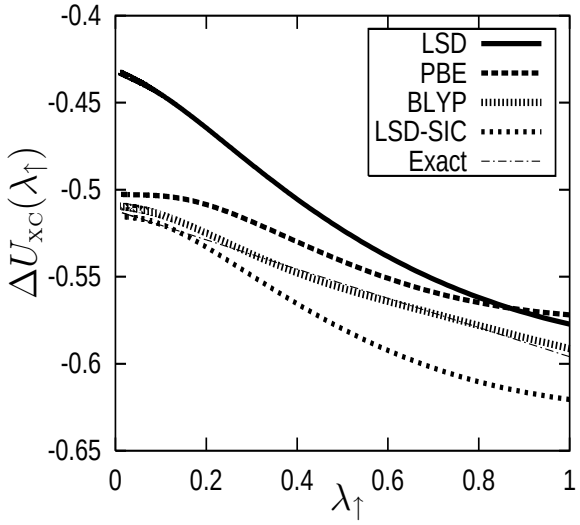

Figure 2.6: Single spin adiabatic connection for a He atom: local spin-density approximation (solid line), generalized gradient approximation (PBE, dashed line), BLYP (bars), self-interaction corrected LSD (short dashes), and exact (dash dot).

	LSD	PBE	SIC	BLYP	"exact"
$\Delta U_{\rm XC}(0)$	-0.43	-0.50	-0.53	-0.51	-0.51
$\Delta U_{\rm XC}(1)$	-0.58	-0.57	-0.62	-0.59	-0.60
$\Delta E_{\rm XC}$	-0.54	-0.54	-0.57	-0.55	-0.56

Table 2.3: Spin adiabatic connection $\Delta U_{\rm XC}(\lambda_\uparrow)$ for He atom, both exactly and in several approximations.

show the spin adiabatic connection for the He atom in Fig. 2.6. In generating each adiabatic connection plot, we now take the scaled spin density to the high density limit (as $\lambda \to 0$). Note this is opposite to the earlier sections. For a given approximation, $\Delta E_{\rm XC}$ is given by the area under each curve. To get $E_{\rm XC}[n_\uparrow, n_\downarrow]$, we must add the contribution from the unscaled spin, $E_{\rm XC}[0, n_\downarrow]$. The spin adiabatic connection curve quite strongly resembles the adiabatic connection curve of total density scaling. The difference being that, for the He atom, $\Delta U_{\rm XC}(\lambda_\uparrow)$ becomes more negative with λ everywhere and is almost linear. This suggests that the spin-correlation effects are weak for this system, just as the correlation effects are.

To better understand how popular approximations perform, comparisons to the exact curve are necessary. This requires sophisticated wavefunction calculations designed to generate the exact spin-scaled densities at every point in the adiabatic connection curve. Here, we use a simple interpolation that should be highly accurate. Analytic formulae give exact limits for $\Delta U_{\rm XC}(\lambda_\uparrow)$. In the limit of small $\lambda_\uparrow$, exchange dominates, and the exchange contribution from the scaled spin to the total energy remains:

$$\Delta U_{\rm XC}(\lambda_\uparrow = 0) = \frac{1}{2} E_{\rm X}[n] \tag{2.28}$$

In the physical limit,

$$\begin{aligned} \Delta U_{\rm XC}(\lambda_\uparrow = 1) = 2E_{\rm XC}[n_\uparrow, n_\downarrow] - 2E_{\rm XC}[0, n_\downarrow] \\ -dE_{\rm XC}[n_{\uparrow\alpha}, n_\downarrow]/d\alpha|_{\alpha=1} \end{aligned} \tag{2.29}$$

For a spin-unpolarized two electron system like the He atom, this becomes

$$\begin{aligned} \Delta U_{\rm XC}(\lambda_\uparrow = 1) = E_{\rm X}/2 + 2E_{\rm C} - (E_{\rm C} + T_{\rm C})/2 \\ (2 \text{ electrons, unpol.}) \end{aligned} \tag{2.30}$$

For He at $\lambda_\uparrow = 1$, $\Delta U_{\rm XC}(\lambda_\uparrow) = -0.60$. To approximate the exact curve, we use a (1,1) Padé approximant. The values $\Delta U_{\rm XC}(0)$, $\Delta U_{\rm XC}(1)$, and $\Delta E_{\rm XC}$ fix the three

unknown parameters. This Padé approximation turns out to be nearly a straight line.

Table 2.3 shows a comparison of the exact limits and those given by some popular functionals. BLYP reproduces both limits most accurately and is mostly linear. This should not be surprising as BLYP yields good energies and accounts for He's self-interaction error. Such good results are not expected when the BLYP functional is applied to the Li atom. As we have seen in the previous section, BLYP predicts zero correlation energy even when two electrons remain in the unscaled spin channel. The LSD functional dramatically underestimates the single spin exchange energy and, therefore, gets the small $\lambda_\uparrow$ limit quite wrong. This reflects the usual error for LDA exchange. But notice how well LSD performs performs at $\lambda_\uparrow = 1$. The value here is only a 3% overestimate of the exact value, much better than the 9% overestimate for the exchange-correlation energy. Furthermore, the LSD derivative as $\lambda_\uparrow \to 1$ is almost exact. PBE and LDA-SIC are qualitatively similar, the greater error in LSD-SIC being due to the errors in LSD. Both show a flattening of the curve as $\lambda_\uparrow \to 0$, much more than BLYP. Our "exact" curve is too crudely constructed to indicate which behavior is more accurate.

Ideally, comparison to the exact adiabatic connection plot, if available, would be made. Even so, analyses of exact limits are sufficient to garner a deeper understanding of how functionals treat spin densities.

2.6 Conclusions

The scaling method and the adiabatic decomposition formula have proven extremely useful in studying and constructing total density functionals. We have investigated the scaling of spin densities separately, derived a new virial theorem within this spin scaling formalism, (Eq. (2.12)) shown exact results for the

He atom, derived a spin-adiabatic connection, and indicated the difficulties of deducing exact theorems from this decomposition. While exact calculations are difficult to perform and exact results somewhat difficult to obtain within this approach, any result is useful and likely to improve spin density functional theory's treatment of magnetic properties.

We close with a significant challenge to developing separate spin scaling. In the total density scaling of Eq. (1.16), the density is both squeezed (or spread) and is also translated. The squeezing is independent of the choice of origin, but the translation is not. This origin-dependence should not affect the exchange-correlation energy because space is translationally invariant. However, when an individual *spin* density is scaled, the remaining spin density remains fixed in space. This means the resulting density depends on the choice of origin for the separate spin-scaling. So while $E_{\rm C}[n_{\uparrow\alpha}, n_{\downarrow}]$ is a spin-density functional of $n_{\uparrow\alpha}$ and $n_{\downarrow}$, it is *not* a pure spin-density functional of the original spin-densities because of this origin dependence. Most likely, a method of transforming away this origin dependence, as found for virial energy densities in Ref. [44], will be needed to make this spin scaling technique more physical and useful. For atoms, we made the obvious choice of origin at the center of the nucleus. Origin dependence will become acute in applications to molecules and even worse for solids. On the other hand, the non-uniform coordinate scaling of Görling and Levy [45] suffers from the same difficulties for non-spherical densities but has still produced useful limits for approximate density functionals [46].

However, it is important to stress that the spin virial relationship equation, (2.12), is unaffected by this challenge. For α arbitrarily close to 1, the spin-scaled energies are independent of the choice of origin, and these difficulties are irrelevant. The spin virial relationship is an exact constraint and gives us a useful measure of how the correlation energy is affected by small changes in the spin densities. It also leads to a natural decomposition of energy changes due to

separate spin densities. It should be useful in determining whether calculations are self-consistent for each spin density separately. This might be useful for example in systems where small differences between spin densities are important to calculate properly.

Chapter 3
Correlation Energies in the High Density Limit

It is important to consider functional behavior of various quantities in different limits to provide constraints for functional development. In the previous chapter, we primarily explored the correlation energy under spin scaling to the low density limit (i.e. as the density of one spin channel is scaled away by a scale factor approaching zero while that of the other spin channel remains unscaled). Here, we investigate correlation energies as they are scaled to the high density limit. In this limit, the scale factor becomes infinitely large, the length scale shrinks, and the density becomes hydrogenic. We expand the density, potential, and correlation energies to second order in the inverse scale factor and extract the coefficients for each quantity for various ions. This expansion provides yet another constraint of proper scaling behavior; thus any given correlation functional can be tested for proper behavior in this limit.

There are quantum chemistry benchmarks for correlation energies of various isoelectronic series,[49, 50] i.e. sets of ions with the same numbers of electrons. Such benchmarks do not exist for DFT despite their potential usefulness. In this chapter we consider the behavior of the correlation energy in the high density limit when the nuclear charge, Z, becomes infinitely large. In many ways, the effect is similar to that of scaling in DFT.

One important difference between the coordinate scaling and scaling by increasing the nuclear charge of ions is the change in the shape of the density with Z. These changes must be accounted for and are the correction terms to the

usual scaling expansion coefficients when relating them to the coefficients of scaling in Z. It would be useful to have benchmarks on hydrogenic densities because the ability of functionals to reproduce these benchmarks is a means of testing their accuracy in the high density limit. There is a beautiful simplification of the expression of the high-Z correlation coefficients in terms of the Görling-Levy coefficients when the sum of kinetic and total correlation energies is considered. This makes the method more easily applicable for testing.

Herein we determine, to second order in $1/Z$, the expansion coefficients of the correlation energy for non-degenerate ions, the density coefficients for $N = 2, 3$, and 10-electron ions, and the correlation potential coefficients for $N = 2$-electron ions. The correlation energy coefficients were determined by a least squares fit to correlation energy data reported in the literature.[49, 50] The density coefficients were obtained from exact exchange calculations using Engel's atomic DFT code.[51] Finally, the correlation potential coefficients were extracted from Umrigar's quantum monte carlo (QMC) calculations for 2-electrons.

For non-degenerate systems, the correlation energy scales to a constant. [139] Not all approximate correlation functionals scale correctly to the high-density limit. The local density approximation (LDA) violates this condition. The long-range nature of the Coulomb interaction in an infinite system (the uniform electron gas) leads to a logarithmic divergence.[17] The parametrization of the PW91 functional [17] fails to capture the correct behavior, but the PBE correlation functional was designed to correct this.[18] The PBE functional yields good results for the correlation energy of these large Z atoms.

3.1 Scaling in the high density limit

Scaling to the high-density limit is particularly simple in DFT, and a perturbation theory has been developed to take advantage of it. Görling and Levy [215] have

shown that

$$\lim_{\gamma\to\infty} E_{\rm C}[n_\gamma] = E_{\rm C}^{(2)}[n] + \frac{1}{\gamma}E_{\rm C}^{(3)}[n] + \frac{1}{\gamma^2}E_{\rm C}^{(4)}[n] + ... \tag{3.1}$$

where each $E_{\rm C}^{(p)}[n]$ is a *scale-independent* functional, i.e, $E_{\rm C}^{(p)}[n_\gamma] = E_{\rm C}^{(p)}[n]$.

It would be natural to equate γ above with Z in large-Z atoms, as both quantities perform the same under dimensional analysis and many functions tend to the same value as either Z or $\gamma \to \infty$. But a crucial difference is that in coordinate scaling, the density does not change shape, while as $Z \to \infty$, it does. We show below that this difference is irrelevant at zero-order, but requires careful treatment for all orders beyond that.

3.2 Large Z atoms

We consider the behavior of ions of fixed electron number N, as $Z \to \infty$. Results for these systems are well-known [49, 50] in wavefunction theory, for many values of Z. Many quantities can be expanded as a function of $1/Z$, once their large Z behavior is understood. We consider only those atoms that do not exhibit degeneracies in the $Z = \infty$ limit. For all others, Davidson shows that in the high Z limit, the energy for these atoms becomes degenerate and the correlation energy does not approach a constant. [152]

Begin with the correlation energy. For atoms whose outermost electron is in a non-degenerate orbital, the quantum-chemical correlation energy, defined as the difference between an exact non-relativistic quantum mechanical ground-state energy and a Hartree-Fock energy, tends to a finite limit as $Z \to \infty$. Thus we may write

$$E_{\rm C}(Z) = E_{\rm C}^{[0]} + \frac{E_{\rm C}^{[1]}}{Z} + \frac{E_{\rm C}^{[2]}}{Z^2} + ... \qquad\qquad Z \to \infty \tag{3.2}$$

We use superscript square brackets to denote powers of $1/Z$. The DFT definition of the correlation energy is via a minimization over all slater determinants arising from a one-body potential that yield the same density, thus its magnitude is

Table 3.1: Correlation energy coefficients of 1/Z expansion in mH for select electron number, N.

N	$E_{\rm C}^{[0]}$	$E_{\rm C}^{[1]}$	$E_{\rm C}^{[2]}$
2	-46.68	9.98	-1.4
3	-53.62	25.1	-0.6
7	-236.9	353	-93
8	-306.0	446	-210
9	-369.1	521	-540
10	-428.2	601	-1400
11	-460.2	793	-900

smaller than that of quantum chemistry. The difference between quantum chemistry and density functional correlation energies is generally small,[58] and for the purposes of this paper we ignore the difference.

The best numbers that we use are from Umrigar's QMC calculations for $N = 2$ ions. We compare Davidson's numbers for these 2-electron ions and confirm that, as expected, there is no difference. This justifies use of Davidson's data for other N-electron ions.

Table 3.1 lists the coefficients of the high Z correlation energy expansion for various atoms. These were determined by a quadratic least squares fit of correlation energy as a function of inverse nuclear charge data. [49, 50] The leading term, $E_{\rm C}^{[0]}$, is an extrapolation to $1/Z = 0$ and is the most accurate term given in the table. The numbers agree with data previously published in Refs., [59, 60] the only exception being $E_{\rm C}^{[0]}$ for the sodium isoelectronic series. It is clear from an extrapolation of the best fit to the data that the correlation energy is not -453.4 mH at $1/Z = 0$ as previously reported (see Fig 3.1). We believe that our estimate of $E_{\rm C}^{[0]}$ for 11-electron atomic ions is more accurate. The accuracy of our predicted coefficients decreases with order, with a large uncertainty for the second order correction term, $E_{\rm C}^{[2]}$.

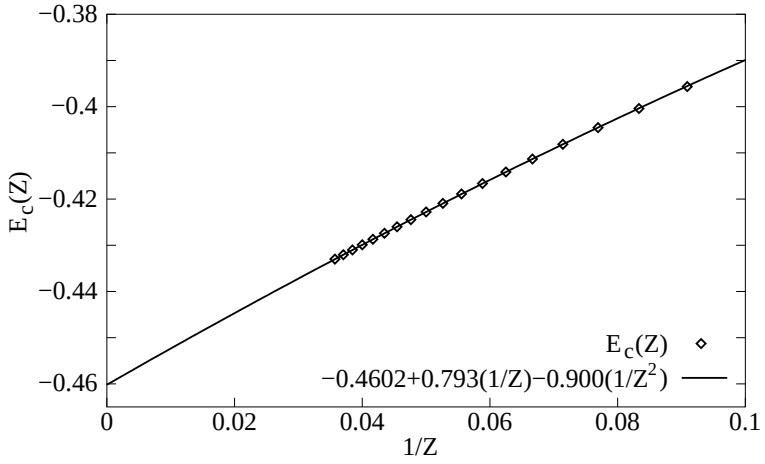

Figure 3.1: Determination of correlation energy coefficients in $1/Z$ for the sodium isoelectronic series.

The density can also be expanded in powers of $1/Z$:

$$n(Z;\mathbf{r}) = Z^3 \left\{ n_{\mathrm{H}}(Z\mathbf{r}) + \Delta n^{[1]}(Z\mathbf{r})/Z + \Delta n^{[2]}(Z\mathbf{r})/Z^2 + ... \right\} \tag{3.3}$$

the leading term being the density of a Hydrogenic atom with N electrons. The quantities $n_{\mathrm{H}}(\mathbf{r}), \Delta n^{[1]}(\mathbf{r})$, and $\Delta n^{[2]}(\mathbf{r})$ are all independent of Z and finite.

We calculated these using Engel's numerical atomic code [51] that calculates energies and other quantities for atoms using density functional methods. For our calculation of the densities, we use exact exchange only. This yields the hydrogenic density and the first correction term, $\Delta n^{[1]}(\mathbf{r})$, exactly, and gives a very accurate second order correction term in comparison to Umrigar's data for $N = 2$ (see Fig. 3.2). Figures 3.3 through 3.5 show the expansion coefficients for the helium, lithium, and neon isoelectronic densities. The corrections to the hydrogenic densities get comparatively larger as the number of electrons increases.

Lastly, we extract the large-Z limit expansion of the correlation potential:

$$v_{\mathrm{C}}[n](Z;\mathbf{r}) = v_{\mathrm{C}}^{[0]}(Z\mathbf{r}) + \frac{v_{\mathrm{C}}^{[1]}(Z\mathbf{r})}{Z} + \frac{v_{\mathrm{C}}^{[2]}(Z\mathbf{r})}{Z^2} + ... \qquad Z \to \infty. \tag{3.4}$$

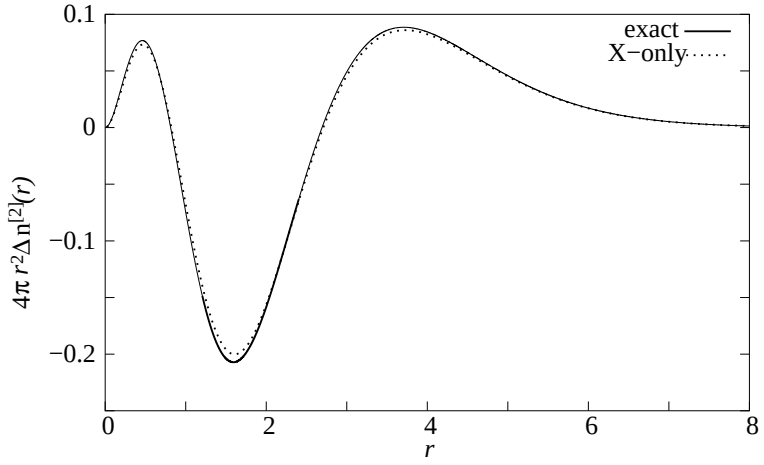

Figure 3.2: Second order correction to the density, $\Delta n^{[2]}$, for 2-electron ions. The solid line is the exact curve extracted from Umrigar's data.[37, 151] The dashed line is the self-consistent exact exchange-only result.[51]

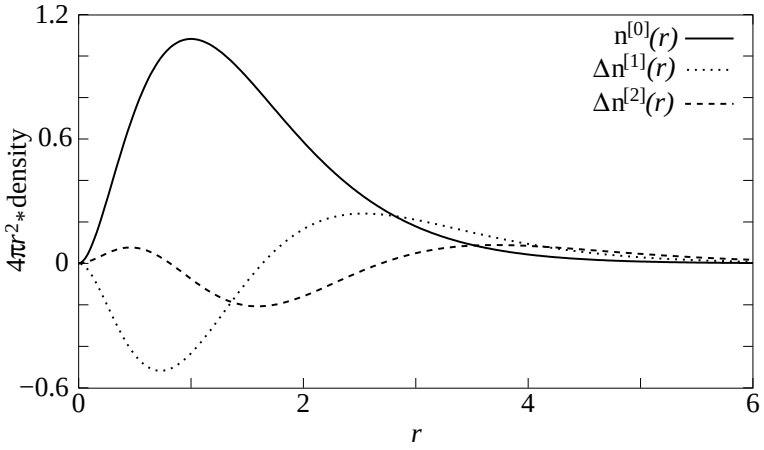

Figure 3.3: Coefficients of density expansion in 1/Z for the helium isoelectronic series: the leading term (the hydrogenic density for 2 electrons) (solid line), the coefficient of the leading correction (short dashes), and the coefficient of the second order correction (long dashes).

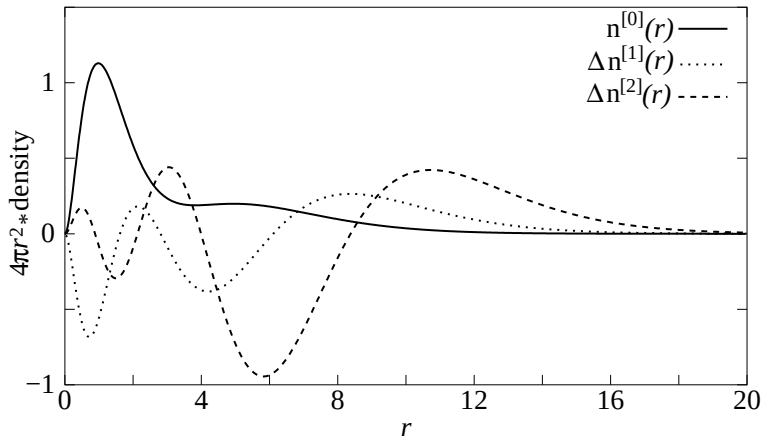

Figure 3.4: Same as Fig. 2, but for the lithium isoelectronic series.

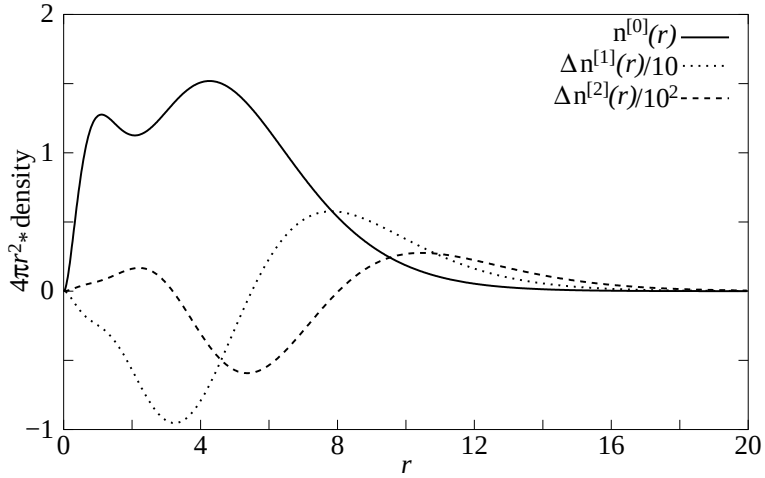

Figure 3.5: Same as Fig. 2, but for the neon isoelectronic series.

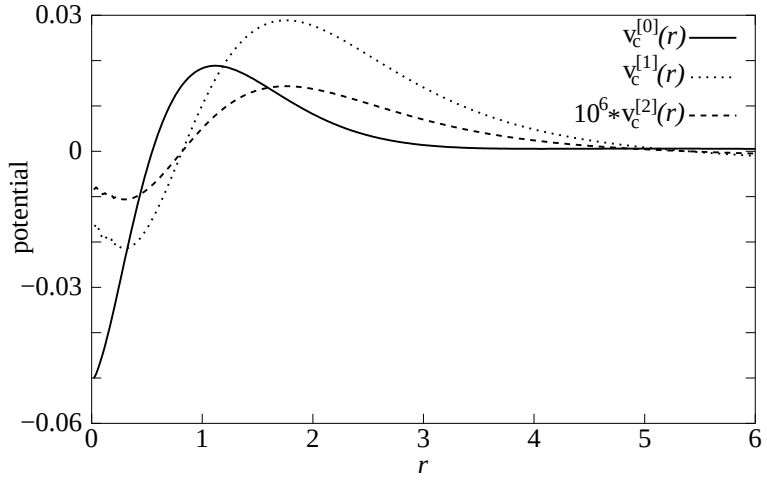

Figure 3.6: Expansion coefficients for Umrigar's correlation potential for the helium isoelectronic series: the leading term, $v_{\rm C}^{[0]}(\mathbf{r})$ (solid line), the coefficient of the first order correction term, $v_{\rm C}^{[1]}(\mathbf{r})$ (short dashes), the coefficient of the second order correction term, $v_{\rm C}^{[2]}(\mathbf{r})$ (long dashes).

Figure 3.6 shows the large-Z limit expansion coefficients of the correlation potential for the helium isoelectronic series.

3.3 Relation between different limits

In this section, we carefully derive the relationships between the large Z expansion and the high-density limit of density functional theory. In addition to the expansion of the energy and density, we also need the expansion of the correlation potential, $v_{\rm C}[n(Z;r)]$. From the definition of the functional derivative, one can show:

$$v_{\rm C}[n_\gamma](\frac{\mathbf{r}}{\gamma}) = \frac{\delta E_{\rm C}[n_\gamma]}{\delta n(\mathbf{r})} \tag{3.5}$$

Thus, in the high density limit, from Eq. (3.1),

$$\begin{aligned} v_{\rm C}[n_\gamma](\frac{\mathbf{r}}{\gamma}) &= \frac{\delta E_{\rm C}^{(2)}[n]}{\delta n(\mathbf{r})} + \frac{1}{\gamma}\frac{\delta E_{\rm C}^{(3)}[n]}{\delta n(\mathbf{r})} + ... \quad \gamma \to \infty \\ &= v_{\rm C}^{(2)}[n](\mathbf{r}) + \frac{1}{\gamma} v_{\rm C}^{(3)}[n](\mathbf{r}) + ... \end{aligned} \tag{3.6}$$

Applying this expansion to the large Z limit, we obtain

$$\begin{aligned} v_{\rm C}(Z;\frac{\mathbf{r}}{Z}) &= v_{\rm C}[(n_{\rm H}(\mathbf{r})+\frac{1}{Z}\Delta n^{[1]}(\mathbf{r})+...)_Z]\left(\frac{\mathbf{r}}{Z}\right) \\ &= v_{\rm C}^{(2)}[n_{\rm H}+\frac{1}{Z}\Delta n^{[1]}](\mathbf{r})+\frac{1}{Z}v_{\rm C}^{(3)}[n_{\rm H}](\mathbf{r})+... \end{aligned} \tag{3.7}$$

Take the limit to get

$$\begin{aligned} \lim_{Z\to\infty} v_{\rm C}[n(Z;\mathbf{r})]\left(\frac{\mathbf{r}}{Z}\right) = v_{\rm C}^{(2)}[n_{\rm H}](\mathbf{r})+\frac{1}{Z}\Big\{ v_{\rm C}^{(3)}[n_{\rm H}](\mathbf{r}) \\ +\int d^3r'\Delta n^{[1]}(\mathbf{r})\ f_c^{(2)}[n_{\rm H}](\mathbf{r},\mathbf{r}')\Big\}+... \end{aligned} \tag{3.8}$$

where $f_{\rm C}^{(2)}[n](\mathbf{r},\mathbf{r}')$ is the second functional derivative of the leading term in the GL expansion, $E_{\rm C}^{(2)}[n]$. We deduce:

$$v_{\rm C}^{[0]}[n_{\rm H}](\mathbf{r}) = v_{\rm C}^{(2)}[n_{\rm H}](\mathbf{r}) \tag{3.9}$$

and

$$v_{\rm C}^{[1]}[n_{\rm H}](\mathbf{r}) = v_{\rm C}^{(3)}[n_{\rm H}](\mathbf{r})+\int d^3r'\Delta n^{[1]}(\mathbf{r})\ f_c^{(2)}[n_{\rm H}](\mathbf{r},\mathbf{r}') \tag{3.10}$$

Thus the leading term in the corrlation potential as $Z\to\infty$ is exactly the high-density limit of the correlation potential of the hydrogenic density, but this is not true for the first correction.

We are ready to deduce formulas for the coefficients of the $1/Z$-expansion in Eq. (3.2).

$$E_{\rm C}^{[0]} = \lim_{Z\to\infty} E_{\rm C}[Z^3 n_{\rm H}(Z\mathbf{r})+...] = E_{\rm C}^{(2)}[n_{\rm H}] \tag{3.11}$$

This shows that, in the high density limit, the correlation energy approaches the GL second-order correlation energy coefficient, evaluated on the hydrogenic density for a given number of electrons. Similarly,

$$E_{\rm C}^{[1]} = \lim_{Z\to\infty} Z(E_{\rm C}(Z)-E_{\rm C}^{[0]}). \tag{3.12}$$

Expanding $n(Z;r)$ around $n_{H,Z}(\mathbf{r})$, the hydrogenic density, substituting, and taking the limit, we obtain

$$E_{\rm C}^{[1]} = E_{\rm C}^{(3)}[n_{\rm H}]+\int d^3r\Delta n^{[1]}(\mathbf{r})\ v_{\rm C}^{(2)}[n_{\rm H}](\mathbf{r}). \tag{3.13}$$

Thus the next terms in the two expansions *differ*, due to the change in shape of the density. Continuing to the next order, we find several corrections:

$$\begin{aligned} E_{\rm C}^{[2]} = E_{\rm C}^{(4)}[n_{\rm H}] + \int d^3r \Delta n^{[1]}(\mathbf{r})\ v_{\rm C}^{(3)}[n_{\rm H}](\mathbf{r}) \\ + \int d^3r \Delta n^{[2]}(\mathbf{r}) v_{\rm C}^{(2)}[n_{\rm H}](\mathbf{r}) \\ + \frac{1}{2}\int d^3r \int d^3r' \Delta n^{[1]}(\mathbf{r})\ \Delta n^{[1]}(\mathbf{r}')\ f_{\rm C}^{(2)}[n_{\rm H}](\mathbf{r},\mathbf{r}') \end{aligned} \tag{3.14}$$

To second order, the correlation energy is a sum of GL correlation energy coefficients evaluated on the hydrogenic density and integrals over their derivatives and corrections to the hydrogenic density. In density functional terms, changes in $E_{\rm C}$ due to changes in nuclear charge are accompanied by changes in the electronic density.

Next we discuss how further information can be extracted from highly accurate quantum calculations on atoms for large Z, if another key quantity is available. The kinetic contribution to the correlation energy, $T_{\rm C}$, is defined as the difference between the kinetic energy of the physical system, T, and that of the Kohn-Sham system, $T_{\rm S}$. This quantity is not usually calculated by standard codes. In fact, $T_{\rm C}$ can be extremely demanding to calculate, as it involves a small difference between two large numbers. In particular, one needs the non-interacting kinetic energy of the Kohn-Sham orbitals corresponding to the exact density. The kinetic energy of a Hartree-Fock calculation will yield a good approximation, but not good enough for reliable values for $T_{\rm C}$. Fortunately, Umrigar has calculated $T_{\rm C}$ for the two-electron series for many values of Z.

We can write expressions for the high density limit expansion of $T_{\rm C}$ similar to those of $E_{\rm C}$ in sections 3.2 and 3.3. Thus $T_{\rm C}[n]$ may be expanded in the high-density limit in terms of scale-independent functionals $T_{\rm C}^{(p)}[n]$, as in Eq. (3.1); or $T_{\rm C}(Z)$ can be expanded around $Z \to \infty$ in terms of $T_{\rm C}^{[p]}$, as in Eq. (3.2). If we define its potential by

$$v_{T_{\rm C}}[n](\mathbf{r}) = \frac{\delta T_{\rm C}[n]}{\delta n(\mathbf{r})} \tag{3.15}$$

and expand it around $Z \to \infty$, we find analogs of Eqs. (3.11), (3.13), and (3.14), relating the two expansions for $T_{\rm C}$.

However, the kinetic correlation and correlation energies are related by scaling:[38]

$$\gamma \frac{dE_{\rm C}[n_\gamma]}{d\gamma} = E_{\rm C}[n_\gamma] + T_{\rm C}[n_\gamma] \tag{3.16}$$

Expanding Eq. (3.16) around $\gamma \to \infty$, we determine that the high-density limit of the kinetic contribution is simply:

$$T_{\rm C}^{(p)}[n] = -(p-1)E_{\rm C}^{(p)}[n] \qquad\qquad p = 2, 3, 4, ... \tag{3.17}$$

and that

$$v_{T_{\rm C}}^{(p)}[n](r) = -(p-1)v_{\rm C}^{(p)}[n](r). \tag{3.18}$$

Particularly useful is the fact that $v_{T_{\rm C}}^2[n] = -v_{\rm C}^2[n]$, so that the potential corrections to $E_{\rm C}^{[1]} + T_{\rm C}^{[1]}$ cancel, yielding

$$E_{\rm C}^{[1]} + T_{\rm C}^{[1]} = E_{\rm C}^{(3)} + T_{\rm C}^{(3)} = -E_{\rm C}^{(3)}[n_H], \tag{3.19}$$

that is, expansion of $E_{\rm C} + T_{\rm C}$ in powers of $1/Z$ yield $E_{\rm C}^{(3)}[n_H]$ directly. Similarly all integrals with potentials of order (2) in the next order term cancel, yielding

$$E_{\rm C}^{[2]} + T_{\rm C}^{[2]} = -2E_{\rm C}^{(4)} - \int d^3r \Delta n^{[1]}(\mathbf{r}) v_{\rm C}^{(3)}[n_H](\mathbf{r}), \tag{3.20}$$

a less useful result.

The high density limit expansion was first tested on the helium isoelectronic series for which Umrigar *et.al.* [37, 150, 151] have calculated exact values for the density and potential as well as $E_{\rm C}$ and $T_{\rm C}$. The components necessary to evaluate $E_{\rm C}(Z) + T_{\rm C}(Z)$ were extracted. When compared, the correlation energy terms for the helium isoelectronic series extracted using data from Davidson's exact calculations correspond well with those of Umrigar (Table 3.5).

One can also write a virial expression for $E_{\rm C}[n] + T_{\rm C}[n]$:

$$-\int d^3r \; n(\mathbf{r}) \; \mathbf{r} \cdot \nabla v_{\rm C}(\mathbf{r}) = E_{\rm C}[n] + T_{\rm C}[n] \tag{3.21}$$

This virial may also be expanded in $1/Z$ to give a leading term:

$$-\int d^3r\ n_H(\mathbf{r})\ \mathbf{r}\cdot\nabla v_{\rm C}^{(2)}[n_H](\mathbf{r}) = 0 \tag{3.22}$$

and a first order correction:

$$-\int d^3r\Big\{n_H(\mathbf{r})\mathbf{r}\cdot\nabla v_{\rm C}^{[1]}(\mathbf{r}) + \Delta n^{[1]}(\mathbf{r})\mathbf{r}\cdot\nabla v_{\rm C}^{[0]}(\mathbf{r})\Big\} = E_{\rm C}^{[1]} + T_{\rm C}[1]. \tag{3.23}$$

This first order virial correction may be written in terms of GL coefficients:

$$\int d^3r\Big\{n_H(\mathbf{r})\mathbf{r}\cdot\nabla v_{\rm C}^{(3)}(\mathbf{r}) + \Delta n^{[1]}(\mathbf{r})\mathbf{r}\cdot\nabla v_{\rm C}^{(2)}(\mathbf{r})\Big\} = E_{\rm C}^{(3)}[n_H]. \tag{3.24}$$

The kinetic correlation may also be expressed in terms of a virial of total correlation potentials and derivatives:

$$\begin{aligned} v_{T_{\rm C}}[n](\mathbf{r}) = \ &- \ \mathbf{r}\cdot\nabla v_{\rm C}[n](\mathbf{r}) - \int d^3r\ \mathbf{r}\cdot\nabla f_{\rm C}[n](\mathbf{r},\mathbf{r}') \\ &- \ v_{\rm C}[n](\mathbf{r}) \end{aligned} \tag{3.25}$$

3.4 Neutral atoms

In this last section, we use insight gained from the exact large Z limit to deduce approximate results for $Z = N$, thereby demonstrating that such studies have practical as well as methodological implications.

Correlation energies for a few atoms are listed in Table 3.4. The correlation energy is consistently underestimated by the Morrison and Zhao [40](MZ) estimate, which are determined from configuration interaction calculated reference densities using Slater type orbital basis sets. [50, 62, 63] The MZ estimate is good for small electron number, but its error consistently increases with electron number. This indicates the difficulty in calculating correlation energies rather than correlation energy differences. Our expansion-constructed correlation energy is an extrapolation from the high density limit to the physical ($Z = N$) limit. We take the correlation energy coefficients determined in Table 3.1 and substitute

$Z = N$ into Eq. (3.2). This extrapolated correlation energy gives a surprisingly good approximation for the neutral atoms, with smaller errors than those due to basis sets in the MZ estimate.

As mentioned in the previous section, accurate calculation of $T_{\rm C}$ is very demanding, and only limited results are available in the literature. In particular, Morrison and Zhao used a clever algorithm to construct the exact Kohn-Sham potential and orbitals for the densities discussed above.[147, 191, 222] This produced a list of $T_{\rm C}$ for neutral atoms up to argon.

If we ignore changes in shape of the density, we can approximate $E_{\rm C}[n_\gamma]$ by $E_{\rm C}(Z)$, equating changes with Z with changes with γ. That is, the change in shape of the density caused only a 15% error in the correlation energy first order correction term, $E_{\rm C}^{(3)}$. This method was used by Frydel *et. al.*,[38], but a correction using the potential was used there, making it extremely accurate. The correction is not accessible here, requiring as it does the exchange-correlation potential.

We must still devise a method for choosing the 'best' relation between Z and γ. We know that under exact scaling

$$\gamma = \frac{E_{\rm X}[n_\gamma]}{E_{\rm X}[n]} = \sqrt{\frac{T_{\rm S}(Z*)}{T_{\rm S}(Z)}} \tag{3.26}$$

We can approximate the latter relationship with ease for atomic ions. In a Hartree-Fock calculation, by virtue of the virial theorem,[23] $T^{HF} = -E^{HF} \simeq T_{\rm S}$, where T^{HF} and E^{HF} are the Hartree Fock kinetic and total electronic energies. Thus knowledge of $E^{HF}(Z)$, for fixed N, as reported by Davidson *et. al.* allows us to estimate $\gamma(Z)$ for a given neutral, and Eq. (3.16) then yields $T_{\rm C}$. Figure 3.7 shows $E_{\rm C}[n_\gamma]$ estimated in this way for N=10. Note that, for example, the $\gamma \to \infty$ value differs from $E_{\rm C}^{[0]}$, as this curve approximates $E_{\rm C}[n_\gamma]$ for the neutral atom density. Lastly, in the spirit of Table 3.4, we use the slope as $\gamma \to \infty$, to estimate $E_{\rm C} + T_{\rm C}$ from Eq. (3.16). Clearly, at $\gamma = 1$, the density changes are too

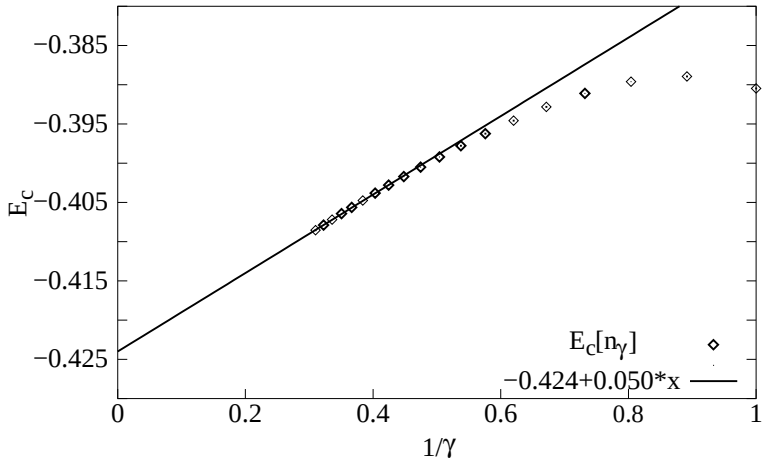

Figure 3.7: Correlation energy of the 10-electron series with γ estimated from Z. The line represents the inital slope and is assumed to be the slope at $\gamma = 1$ when estimating $E_{\mathrm{C}}[n] + T_{\mathrm{C}}[n]$.

Table 3.2: $E_{\mathrm{C}}[n] + T_{\mathrm{C}}[n]$ in mH, where N is the number of electrons.

N	Exact[37, 151]	Extrapolation	MZ[40]	PBE	LYP
2	-5.5	-5.7	-5	-4.3	-9.9
3		-9.0	-7	-4.6	-14.8
7		-50	-30	-22	-64
8		-55	-50	-34	-81
9		-53	-70	-40	-90
10	-65.0	-50	-80	-45	-98
11		-92	-70	-44	-102

great to be accurately estimated by our crude approximation.

There is interesting structure in the $E_{\mathrm{C}} + T_{\mathrm{C}}$ data. In particular, a closer look at extrapolation values in Table 3.2 shows a jump in the magnitude of the correlation energy sum when an electron is placed in a new shell as in going from He to Li and from Ne to Na. In contrast, filling the p orbitals does not appear to be costly. While there is an increase in order of magnitude of correlation, the energy levels off as this subshell is being filled. Trends in the M&Z data are different; there are no marked increases in filling a new shell or subshell.

Table 3.3: $T_{\rm C}[n]$ in mH, where N is the number of electrons.

N	Exact[37, 151]	Extrapolation	MZ[40]	PBE	LYP
2	36.6	36	37	38	34
3		36	38	47	39
7		138	151	161	129
8		199	194	206	184
9		265	237	257	236
10	328.0	332	299	307	286
11		304	311	329	307

Table 3.4: Exact,[49, 50] our expansion constructed, and the Morrison & Zhao [40] correlation energies of neutral atoms in mH.

N	Exact	Extrap	Extrap % error	MZ	MZ % error
2	-42.04	-42.05	< 1	-42.02	< 1
3	-45.33	-45.32	< 1	-45.17	< 1
7	-188.31	-188.4	< 1	-180.5	-4
8	-257.94	-253.6	-2	-244.3	-5
9	-324.53	-317.8	-2	-307.1	-5
10	-390.47	-382.3	-2	-378.9	-3
11	-395.64	-395.5	< 1	-381.1	-4

Table 3.5: Correlation energy coefficients of 1/Z expansion for select XC-functionals in mH, where N is the number of electrons.

N	Method	$E_C^{[0]}$	$E_C^{[1]}$	$E_C^{[2]}$
2	LYP	-55.1	1076	-90276
	PBE	-48.4	5.1	15
	Davidson	-46.7	10.0	-1.4
3	LYP	-99	221	-383
	PBE	-59	2.4	58
	Davidson	-54	25	1
10	LYP	-524	2733	-77818
	PBE	-459	623	4424
	Davidson	-428	601	-1423

Table 3.5 shows the performance of the PBE and LYP correlation functionals in the high density limit. PW91 and LDA do not behave correctly in this limit. LYP correlation is poor at best in this limit. The higher order terms are especially poor. The PBE functional behaves better in this limit, although there is much room for improvement.

In a recent paper, Staroverov *et. al.* show that two conditions must be satisfied for a functional to accurately reproduce the total energy in this limit.[67] The first is that the functional must accurately predict the leading term in the Z-expansion of the exchange energy and the second is that the correlation energy predicted by the functional must scale properly in the high density limit according to Eq. (1.21). Their paper reports the behavior of a number of functionals in this limit.

While this work was being written, we learned of the work of Staroverov *et. al.*.[67] We thank Staroverov *et. al.* for sharing results prior to publication.

Chapter 4

A Computational Study of Rh and Ir Catalysts Using DFT and MO Methods

The previous two chapters presented studies in the area of density functional development. This chapter, as well as the next, involves the application of electronic structure methods to systems of chemical interest.

Alkanes are abundant and inexpensive in nature, but not very reactive. It is useful to find effective catalysts for the conversion of alkanes to alkenes which can then be easily functionalized to create a wealth of compounds. A good catalyst is able to functionalize alkanes by efficient methods such as oxidation and dehydrogenation. Such methods involve oxidative addition reactions to coordinatively unsaturated metal complexes, some of which may even be able to undergo this process twice. The ML_2X (where M=Rh, Ir; L=a tertiary phospine; X=an anionic ligand) group of organometallic catalysts is known to be effective in these processes.

A considerable amount of research has been done to determine whether catalysis proceeds by an oxidative addition/reductive elimination mechanism or via a series of concerted displacements [72, 73]. With the establishment of effective core potentials (ECP) and accurate first principles methods, computational predictions in organometallic chemistry are feasible.

In this chapter, I discuss the ability of electronic structure methods to predict reaction pathways for the oxidative addition of dihydrogen to $M(PH_3)_3Cl, M = Rh, Ir$ complexes. Kinetic and thermodynamic parameters are determined for

these reactions. All calculations involving Ir were done by Margaret Czerw [74].

4.1 Computational Details

In our study, we compared the performances of Møller-Plesset Perturbation Theory to second and fourth orders (MP2,MP4)[75], coupled-cluster single and double excitation method with triple excitations treated non-iteratively (CCSD(T))[13, 14], and the BLYP [34, 35] and B3LYP [20] GGA and hybrid density functionals. These methods are all discussed in chapter 1.

For the Rh and Ir metal atoms, the Hay-Wadt relativistic small-core ECPs with corresponding split valence double-zeta basis sets (LANL2DZ) [76] were used. Within these ECPs the penultimate and valence shell electrons are released for explicit treatment. Third row elements (P,Cl) were described by the Dunning/Huzinaga all-electron, full double-zeta plus polarization function basis sets [77]. Hydrogen atoms that become hydrides in the products were described by the 311G(p) basis set [78] and those in phosphine groups by the 21G basis set [79]. In cases where hydrogens in phosphine groups were replaced by methyls, these methyl hydrogens were described by the STO-3G basis set [80] and the carbons by the Dunning/Huzinaga double-zeta plus polarization basis set (D95d) [77].

Thermodynamic corrections for finite temperature and vibrational zero-point energy corrections calculated from vibrational frequencies were used to convert internal energies to enthalpies (ΔH; T = 298 K, P = 1 atm) [81]. MP4(SDTQ) and CCSD(T) calculations were performed on MP2 optimized geometries and MP2 data was used for conversions to enthalpy. All calculations were done using the GAUSSIAN 98 series of computer programs [15].

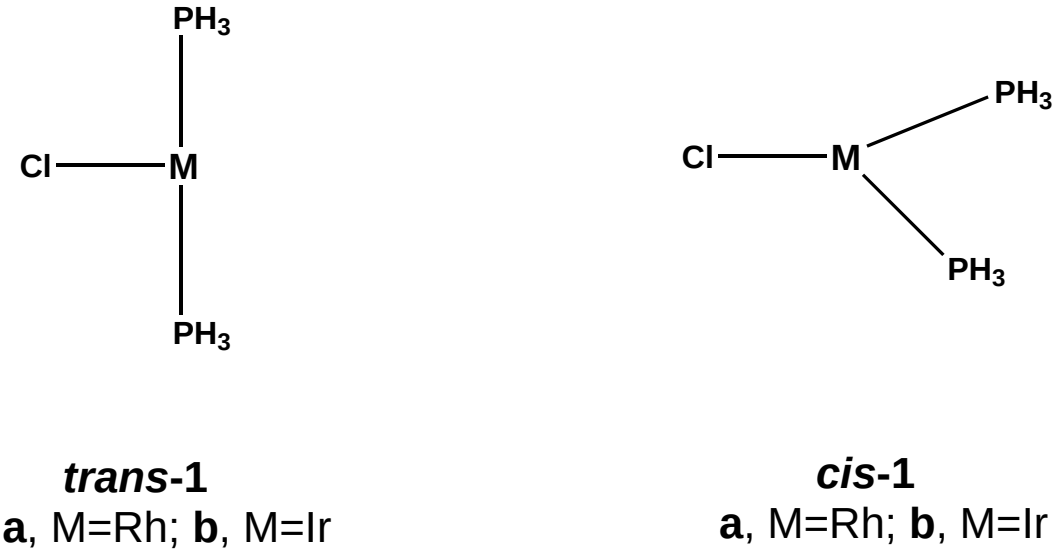

Figure 4.1: Isomers of structure **1**

4.2 Molecular Structures and Spin States of $M(PH_3)_2Cl$, M = Rh and Ir

The two most stable isomers of d^8 metal ML_3 are the trans (T) and cis (Y) structures, all having C_{2v} symmetry [82]. If one ligand is different, other structures become possible. Originally it was believed that the lowest energy conformer was the **trans-1a** structure with Cl at the base of the T [83]. Margl *et. al.* [84] performed calculations which included relativistic energy corrections. They found the energies of triplet and open-shell singlet states for **1a** to be well above those of the closed-shell singlet states. In their density functional study, they calculated the true ground state to be a T-type structure with a phosphine at the base of the T (**cis-1a**, T_{PH_3}), computed to be 16.5 kcal/mol below the T_{Cl} structure. In contrast, Su and Chu [85] report a triplet ground state for **trans-1a**. They did not, however, consider any cis structures.

Our calculations unanimously predict that both **trans-1a** (T_{Cl}) and **cis-1a** (T_{PH_3}) structures of $Rh(PH_3)_2Cl$ exist as discrete minima in singlet states, and

there are no additional minima (Y_{Cl}, etc.). The singlet cis-trans enthalpy difference is calculated to be 10-12 kcal/mol by density functional methods, 14-16 kcal/mol from perturbation theory, and 8.0 kcal/mol from CCSD(T), the most accurate MO method used in this study. The electronic configuration of both structures is $d_{xy}(2)d_{yz}(2)d_{xz}(2)d_{z^2}(2)d_{x^2-y^2}(0)$ where Rh, P, and Cl form the xy plane. In the case of the low-lying triplet state, one electron is promoted from the d_{z^2} orbital to the $d_{x^2-y^2}$ orbital. More than 10 kcal/mol above the singlet state is the triplet **trans-1a** structure which maintains C_{2v} symmetry by the DF methods, but breaks symmetry and collapses to a cis conformation with MP2. All three methods predict planar minima for the triplet **cis-1a**, with the exception being BLYP predicting a slightly pyramidal structure. The **cis-1a** triplet minimum is also higher in energy than the corresponding singlet state (11-13 kcal/mol by DFT, 8-9 kcal/mol by MPn, and 5.6 kcal/mol by CCSD(T)).

The global minimum for $Rh(PH_3)Cl$ is determined by all methods used to be the singlet **cis-1a** (T_{PH_3}) state (Table 4.1). According to the DF methods, the energetic ordering of conformers is as follows: **cis-1a** (singlet) < **trans-1a** (singlet) < **cis-1a** (triplet) < **trans-1a** (triplet), in agreement with Margl *et. al.* [84]. By MO methods, the ordering is slightly different: **cis-1a** (singlet) < **cis-1a** (triplet) < **trans-1a** (singlet). Margl *et. al.* [84] attribute this stability of the cis structures over the trans structures to a larger trans influence exerted by PH_3 relative to Cl [86]. Trans influence is enhanced by covalent metal-ligand interactions and are more pronounced in Ir (see below) which bonds covalently more strongly than Rh.

Now we consider the Ir analog, $Ir(PH_3)_2Cl$, and, not surprisingly, find a potential energy surface that closely resembles that of Rh. Again, the **trans-1b** (T_{Cl}) structure has been extensively studied [85, 87, 88, 89], but a triplet state is found to be lower in energy than the singlet state [85]. In previous work, only the T_{Cl} structure was considered. It was argued that, although a cis-phosphine

Table 4.1: Relative Enthalpies (ΔH, kcal/mol) of $M(PH_3)_2Cl$ (**1**) Species

Species	Isomer	State	BLYP	B3LYP	MP2	MP4(SDTQ)	CCSD(T)
M = Rh							
1a	cis	Singlet	0.0	0.0	0.0	0.0	0.0
1a	cis	Triplet	13.3	10.7	8.4	9.3	5.6
1a	trans	Singlet	11.8	9.9	14.3	15.9	8.0
1a	trans	Triplet	19.4	12.6	[a]		
M = Ir							
1b	cis	Singlet	0.0	0.0	0.0	0.0	0.0
1b	cis	Triplet	20.0	18.5	27.6	23.2	21.0
1b	trans	Singlet	18.3	17.4	26.0	25.4	18.4
1b	trans	Triplet	[a]	23.5	[a]		

[a] The structure collapses to cis; see text.

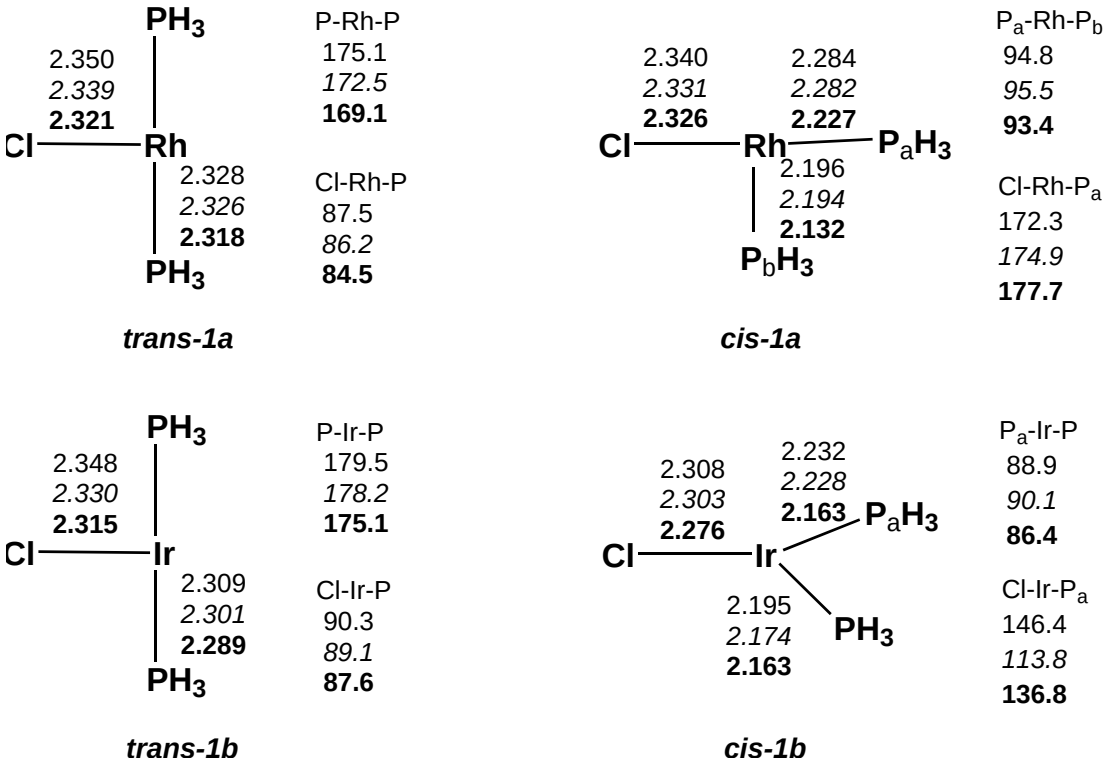

Figure 4.2: k Optimized geometries of $M(PH_3)_2Cl$ isomers, M = Rh and Ir (singlet **trans-1**, singlet **cis-1**). Bond lengths in $\AA$, angles in degrees. BLYP: regular font; B3LYP: *italics*; MP2: **bold**.

structure could exist (Y_{Cl} or T_{PH_3}), for steric reasons a trans conformation would be favorable when the ligands are bulky phosphines (^{t}Bu, ^{i}Pr,Ph, etc.)[88].

In this study, all three methods predict that singlet **trans-1b** and **cis-1b** isomers exist with the global minimum being the singlet, distorted T_{PH_3}-type **cis-1b** structures. The calculated difference in cis-trans enthalpy is 17-18 kcal/mol with DFT, 25-26 kcal/mol at the MP2/MP4 levels, and 18.4 kcal/mol at the CCSD(T) level (Table 4.1).

The **cis-1b** structure, unlike $Rh(PH_3)_2Cl$, distorts towards a Y_{Cl} geometry with the P-Ir-P angle being close to 90°. This deviation from a T geometry is also evidenced by the near equality of the two Cl-Ir-P angles with the largest distortion given by BLYP and the smallest by B3LYP (Fig. 4.2).

MP2 and BLYP predict a collapse of the triplet **trans-1b** to a **cis-1b** structure. The calculated singlet-triplet enthalpy difference for **cis-1b** is approximately 20 kcal/mol by DFT, 23-27 kcal/mol by perturbation theory, and 21.0 kcal/mol by CCSD(T). This large increase in singlet-triplet enthalpy difference may be due to the difference in electronic configurations, the magnitudes of the atomic excitation energies to the lowest doublet states (large in Ir and small in Rh), and the larger ligand field splitting in going from Rh to Ir [90]. The energetic ordering of states is similar to that of **1a**: **cis-1b** (singlet) < **trans-1b** (singlet) < **cis-1b** (triplet) with the global minimum significantly lower than the lowest local minimum in **1b** than in **1a**. As indicated above, Ir bonds covalently and exhibits more trans influence than Rh with a cis-trans enthalpy difference of 18 kcal/mol versus Rh's 8 kcal/mol difference (Table 4.1).

To investigate the argument stated above that bulky phosphine ligands will favor a trans geometry, we performed B3LYP calculations with the hydrogens of the phosphines substituted with methyl groups. The methyl groups model the usual bulky substituents on phosphines required as blocking groups in experiments involving these catalysts. Methyl substituents make the phospines better σ-donors

Table 4.2: Relative Enthalpies (ΔH, kcal/mol) for Dimerization of $M(PH_3)_2Cl$ (Reaction 1) and for H_2 Addition to $M(PH_3)_2Cl$ Species (Reactions 2-4)

Reaction	BLYP	B3LYP	MP2	MP4(SDTQ)	CCSD(T)
M = Rh					
2	-39.1	-43.8	-64.1	[a]	[a]
3	-7.9	-7.9	-21.5	-16.6	-17.9
4	-27.0	-26.2	-46.7	-42.7	-35.0
5	-15.2	-16.3	-32.5	-26.7	-27.0
M = Ir					
2	-40.5	-45.9	-66.7	[a]	[a]
3	-23.6	-25.7	-35.8	-32.6	-36.6
4	-49.0	-51.2	-71.9	-66.9	-64.0
5	-30.7	-33.8	-45.9	-41.5	-45.6

[a] Calculation not attempted.

(more basic) [91], while being computationally manageable.

From our B3LYP calculations we find slightly larger cis-trans energy differences when phosphine hydrogens are replaced with methyls. For $Rh(PMe_3)_2Cl$ the difference is 13.3 kcal/mol and 21.7 kcal/mol for $Ir(PMe_3)_2Cl$. These differences are 3-4 kcal/mol larger than the differences in the parent complexes (10.2 kcal/mol and 17.6 kcal/mol, respectively). When methyls are replaced with tert-butyls, the energetic ordering is reversed and the trans structure (T_{Cl}) becomes more stable by 9.7 kcal/mol. The T_{PH_3} structure, while highly distorted, remains cis (P-Ir-P = 123.3deg, P-Ir-Cl = 98.9deg and 137.0 deg).

There are major experimental difficulties in the application of tricoordinate Rh- and Ir-halide complexes due to thermal (phosphine) degradation and dimer complex formation. The dimerization reaction

$$2M(PH_3)_2Cl \rightarrow (PH_3)_2M(Cl)(Cl)M(PH_3)_2 \tag{4.1}$$

is extremely exothermic (Table 2). The dimerization product (Fig. 4.3) has C_2 symmetry and Cl atoms bridging the metal centers.

In the case of Rh, ΔH = -39.1 kcal/mol (BLYP), -43.8 kcal/mol (B3LYP),

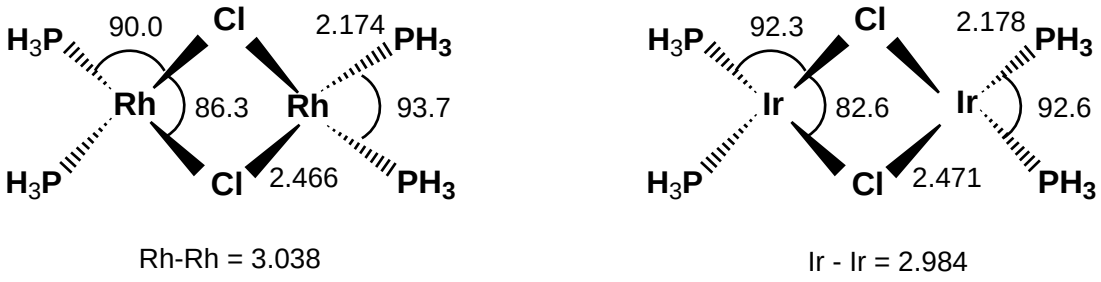

Figure 4.3: B3LYP-optimized geometries of the $(PH_3)_2M(Cl)(Cl)M(PH_3)_2$ dimer. Bond lengths in $\mathring{A}$, angles in degrees.

and -64.1 kcal/mol (MP2). The experimental value for the dimerization enthalpy of $Rh(P^iPr_3)_2Cl$ is -17.4 kcal/mol [92] and provides a lower limit for our calculations. Based on this, a lower limit of 32.5 kcal/mol was calculated for the exothermicity of the hydrogenation reaction $Rh(P^iPr_3)_2Cl + H_2$. The hydrogenation enthalpy was later refined [88] to be up to 39 kcal/mol (i.e. ΔH(H_2 addition) $<$ -39 kcal/mol), which implies that the dimerization enthalpy for $Rh(P^iPr_3)_2Cl$ must exceed 23.9 kcal/mol. Although our results are not in disagreement with experiments, there is cause for concern given the range of predicted dimerization enthalpy [-24 kcal.mol (exp.); -39 kcal/mol to -64 kcal/mol (theory)]. One may conclude that the presence of bulky phosphine and/or solvation significantly affects the dimerization enthalpy. When M = Ir, the dimerization energy is calculated to be 1-2 kcal/mol greater than when M = Rh.

The use of rigid pincer ligands such as tridentate 1,5-bis(dialkylphosphinomethyl)phenyl (PCP) avoids the degradation and dimerization problems stated above. These PCP-based catalysts are stable above 200°C, do not form dimers, and are efficient catalysts for the dehydrogenation of alkanes to form alkenes and dihydrogen [93, 72, 73, 121].

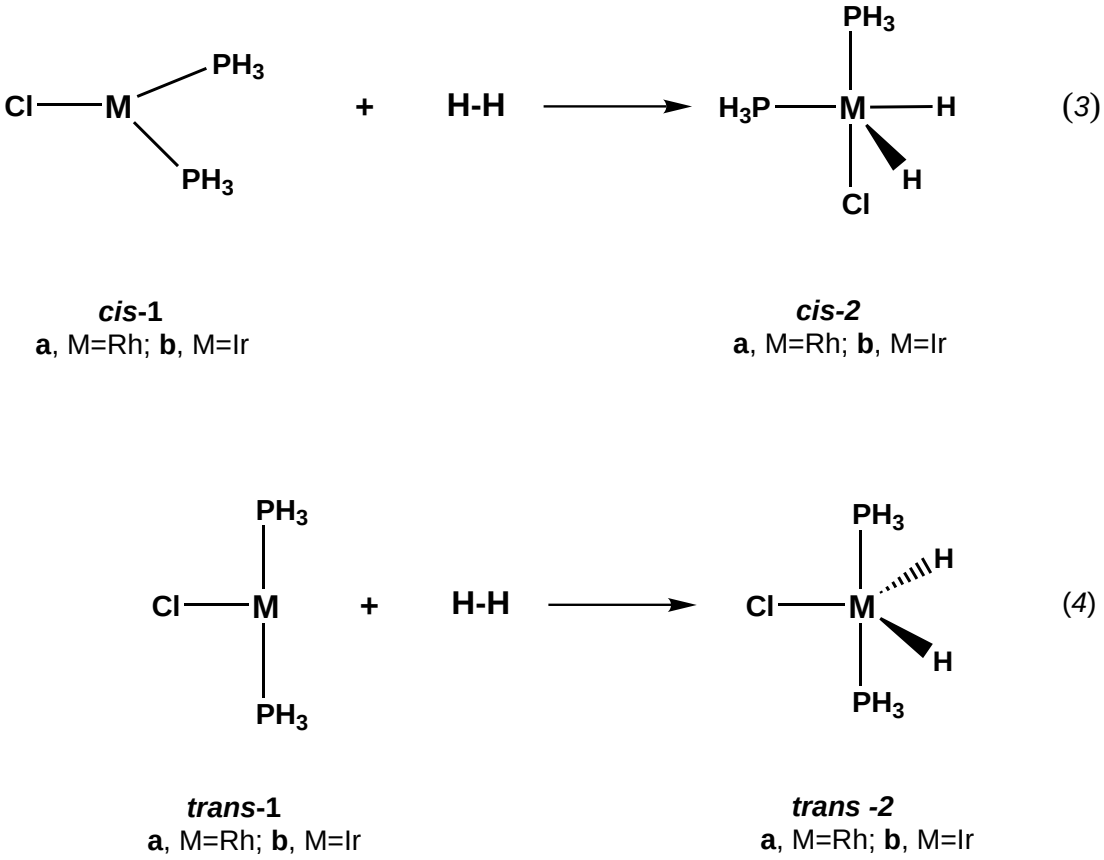

Figure 4.4: Oxidative addition of dihydrogen to M(I) complexes to form M(III) complexes.

4.3 Oxidative Addition of H_2 to $M(PH_3)_2Cl$, M = Rh and Ir: Reaction Products and Transition States

Oxidative addition of dihydrogen to the two singlet conformers of the three-coordinate M(I) complexes (**cis-1**, **trans-1**) identified in the previous section yield M(III) complexes. The **cis-1** reactants form the square pyramidal products (SQP)**cis-2** (reaction 2) whereas the **trans-1** complexes lead to the trigonal bipyramidal (TBP) products **trans-2** (reaction 3).

Addition of dihydrogen to **cis-1a** is exothermic by 8 kcal/mol at the DFT level and more than twice that at the MPn/CCSD(T) levels (Table 4.2). The distorted SQP **cis-2a** product has one hydride apical (Fig. 4.5). Addition to **trans-1a** is

Table 4.3: Relative Enthalpies (ΔH, kcal/mol) of $H_2M(PH_3)_2Cl$ (**2**) Species

Species	Isomer	BLYP	B3LYP	MP2	MP4(SDTQ)	CCSD(T)
M = Rh						
2a	trans	0.0	0.0	0.0	0.0	0.0
2a	cis	7.3	8.4	10.9	10.2	9.1
M = Ir						
2b	trans	0.0	0.0	0.0	0.0	0.0
2b	cis	7.1	8.1	10.0	9.8	8.7

exothermic by 26-27 kcal/mol at the DFT level and more than 40 kcal/mol at the MPn levels; the CCSD(T) value is 35.0 kcal/mol. The TBP **trans-2a** product has a Y_{Cl} shape with a narrow H-Rh-H angle of approximately 62°. All methods used predict that the **trans-2a** structure is approximately 10 kcal/mol lower in enthalpy than **cis-2a** conformer (Table 4.2)[83].

Reaction (3) is 15-18 kcal/mol more exothermic when M = Ir (Table **??**). For reaction (4), when M = Ir the enthalpy is about 25 kcal/mol more exothermic than when M = Rh regardless of method. The **trans-2b** structure is again lower in energy, also regardless of method, with a small H-M-H angle of approximately 65° (Y_{Cl} shape; Fig. 4.5).

A look at the orbitals involved in going from a 14-electron M(I) species to a 16-electron M(III) species shows that this reaction is allowed by orbital symmetry [95] (Fig. 4.6). The LUMO of the three-coordinate species is a hybrid orbital composed of $(n)d_{x^2-y^2}$, (n+1)s, and (n+1)p orbitals extending into the space of the vacant, in-plane coordination site. This orbital has perfect symmetry and orientation to interact with the two electrons in the H_2 σ-bond orbital. Conversely, one of the doubly occupied, in-plane d orbitals (d_{xy}) has the proper pi-type symmetry and extension to interact with the antibonding LUMO of H_2 ($\sigma*$). The formation of the two M-H bonds progresses smoothly as the H-H bond dissociates. The spherical symmetry of the H 1s-orbitals makes it possible not only to achieve

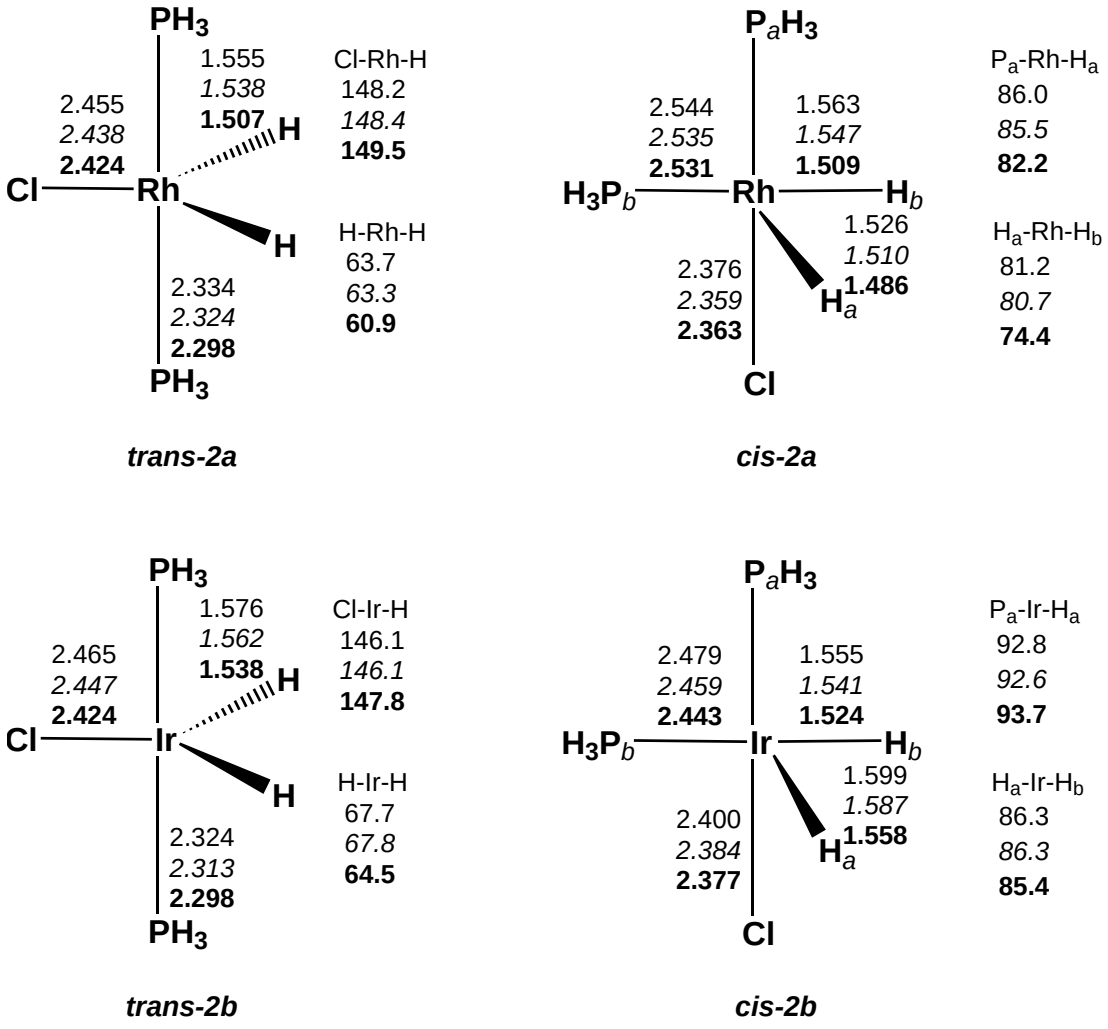

Figure 4.5: Optimized geometries of $H_2M(PH_3)_2Cl$ isomers, M = Rh and Ir (**trans-2**, **cis-2**). Bond lengths in $\AA$, angles in degrees. BLYP: regular font; B3LYP: *italics*; MP2: **bold**.

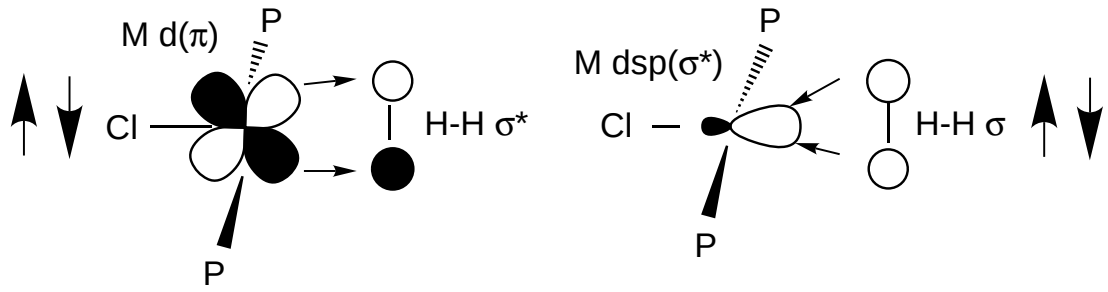

Figure 4.6: Favorable orbital interactions between **1** and H_2

M-H orbital overlap early, and possibly even form a $M(PH_3)_2Cl-H_2$ "precursor" complex, but also to maintain strong overlap throughout the concerted addition process.

LUMO of H_2 ($\sigma*$). This allows for strong overlap and concerted formation of the M-H bonds as the H-H bond dissociates.

As the Hammond principle [96] predicts, there are low or non-existent energy barriers for reactions (3) and (4), and this is clear in their large exothermicities. For M = Ir there are no transition state or precursor structures predicted by any method for reaction (4). It is possible to locate a strongly bound precursor (ΔH -15.5 kcal/mol relative to reactants, H-H = 1.00A) by the B3LYP method only. However, this precursor complex is only 0.3 kcal/mol below the transition state. There does not appear to be an activation energy barrier for the reaction of **1b** and H_2.

At first glance, the situation appears more complex for Rh. Again, for reaction (4), B3LYP predicts a precursor complex (Rh-H = 1.63 A, H-H = 0.96 A) with a binding energy ΔE = -27.6 kcal/mol relative to the reactants. The energy of the transition state is only 0.2 kcal/mol above that of the precursor (Rh-H = 1.58 A, H-H = 1.15 A), and the product (Rh-H = 1.54 A, H-H = 1.61 A) is only 0.8 kcal/mol below the precursor.

All methods predict precursor complexes and/or transition states for the less exothermic reaction (3). B3LYP locates a precursor (Rh-H = 1.75 A, H-H = 0.83 A) with binding energy ΔE = -11.8 kcal/mol with respect to the reactants. B3LYP also finds a transition state 5.7 kcal/mol higher [than the precursor] in energy (Rh-H = 1.56 A and 1.54 A, H-H = 1.32 A), and the **cis-2a** product (Rh-H = 1.51 A and 1.55A, H-H = 1.98 A) is 2.0 kcal/mol higher in energy than the precursor complex. At the MP2 level, only a transition state was found 16.8 kcal/mol below the reactants. These calculations are in the gas phase and neglect dynamics, therefore we do not believe there is an activation barrier for

H_2 addition to **1** (cis or trans) under experimental conditions.

A mix of **cis-1** and **trans-1** isomers would contain mostly the **cis-1** conformer, since it is by far the more stable of the two. It is reasonable to assume that **cis-2** would be the major product of H_2 addition. However, **trans-2** is more stable than **cis-2** by approximately 10 kcal/mol (Table 4.3) and it is conceivable that addition of H_2 may bypass formation of **cis-2**. We identified the transition state for conversion of **cis-2** to **trans-2** to be 10 kcal/mol above **cis-2a** regardless of the metal involved. So this conversion should occur fairly easily and the activation energy is expected to be even lower for bulky phosphine substituents which destabilize **cis-2**.

It seems reasonable to consider reaction enthalpies of lowest energy reactants and products (i.e. **cis-1** and **trans-2**) since this is the overall reaction that takes place (reaction (5) and Table4.2). For $Rh(PH_3)_2Cl$ and M = Rh, the density functional methods predict exothermicities of 15-16 kcal/mol, MPn methods predict 27-32 kcal/mol, and CCSD(T) predicts 27.0 kcal/mol. When M = Ir the exothermicities are more than 15 kcal/mol larger. When the phosphine is methylated (B3LYP only), the exothermicity decreases by 3-4 kcal/mol. The DF methods predict significantly different enthalpies from those predicted by MO methods. For reaction (5), it appears that the DFT-based exothermicities are too low. It is possible that bulky phosphine substituents will destabilize the T_{PH_3} structure and increase the exothermicity of H_2 addition. In the case of Ir, however, the calculated exothermicities (especially the CCSD(T) values) are close to experimental values.

The experimental H_2 bond dissociation enthalpy is 104.2 kcal/mol [97]. The BLYP and B3LYP enthalpies bracket this value at 103.9 kcal/mol and 104.5 kcal/mol, respectively. The MP2/MP4 energies are not as good: 95.2 kcal/mol and 99.9 kcal/mol, respectively, and 100.3 kcal/mol from CCSD(T).

Using the calculated exothermicities of reaction (5), we determine the M-H

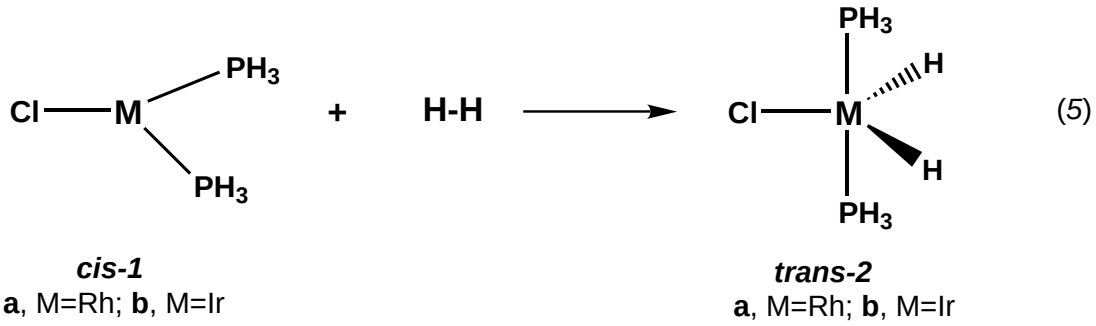

Figure 4.7: Reaction (5): Oxidative addition of dihydrogen to M(i) complex.

bond energies in the **trans-2** product. For M = Rh, we get 59.6 kcal/mol (BLYP), 60.4 kcal/mol (B3LYP), 63.8 kcal/mol (MP2), 63.4 kcal/mol (MP4(SDTQ)), and 63.6 kcal/mol (CCSD(T)). For M = Ir, we get 67.3 kcal/mol (BLYP), 69.2 kcal/mol (B3LYP), 70.1 kcal/mol (MP2), 70.7 kcal/mol (MP4(SDTQ)), and 72.9 kcal/mol (CCSD(T)). The 5d orbitals of Ir extend further than the 4d orbitals of Rh, giving better overlap with ligand orbitals, so the M-H bond strength is enhanced when M = Ir. Close inspection of Fig. 4.2 show that Ir-L bonds tend to be shorter than Rh-L bonds, indicating a stronger bond.

4.4 Oxidative Addition of H_2 to $H_2M(PH_3)_2Cl$, M = Rh and Ir: Reaction Products and Transition States

As discussed in the previous section, the addition of dihydrogen to three-coordinate M(I) complexes to form five-coordinate M(III) complexes proceeds with a small or no barrier. We will now consider addition of a second dihydrogen to form seven-coordinate M(V) polyhydride species. 18-electron seven-coordinate polyhydride complexes are known for Ir(V) but not for Rh(V) [98]. Metals in complexes containing molecular dihydrogen [99] most often have d^6 configuration [100, 101]. Therefore, possible conformers of the seven-coordinate species are: (a) a classical isomer with four M-H bonds, $(H)_4M(PH_3)_2Cl$ (**3**); (b) nonclassical isomers that

have one dihydrogen molecule coordinating cis, $(cis-(H_2)-\eta^2-H_2)M(PH_3)_2Cl$ (**4**), or trans, $(trans-(H_2)-\eta^2-H_2)M(PH_3)_2Cl$ (**5**), to the Cl atom; (c) nonclassical isomers with two dihydrogen molecules coordinated to the metal, $(\eta^2-H_2)_2M(PH_3)_2Cl$ (**6**).

When M = Rh, we are unable to locate isomer **3a** as a minimum. With the BLYP and MP2 methods, **3a** possesses one imaginary frequency and is hence a transition state; at the B3LYP level, the structure is a second-order saddle point. All computational methods predict a minimum corresponding to the nonclassical cis-isomer **4a** (Fig. 4.9). In addition, the DFT methods predict a minimum corresponding to trans-isomer **5a**, whereas MP2 fails to locate a minimum for the tetrahydride. However, the computed **4a-5a** difference is more than 20 kcal/mol (Table 4.4) in favor of **4a**. This result may be yet another manifestation of the strong trans-influence exerted by H, which renders **5a** with two hydrides as a *trans* pair disfavored [86, 102]. Structure **6** appears as a transition state with the B3LYP method; at the BLYP and MP2 levels, any attempt at locating a di-dihydrogen stationary point failed. Although the calculations do not present a fully uniform picture, they clearly favor non-classical over classical structures for $H_4Rh(PH_3)_2Cl$. Lin and Hall have pointed out that the presence of contracted metal d-orbitals will tend to favor the non-classical isomers, where metal-hydrogen electron transfer is minimized [102, 103]. Cis-isomer **4a** is hardly bound relative to **trans-2a** and H_2 with the computed enthalpy for the formation reaction ranging from slightly negative (ΔH = -1.3, -0.5, and -1.2 kcal/mol with MP2, MP4(SDTQ), and CCSD(T), respectively) to positive (ΔH = 2.0 kcal/mol and 2.9 kcal/mol with B3LYP and BLYP, respectively). Since stronger electron donating phosphines favor H_2 addition, it is likely that the formation enthalpies for **4a** will become more negative by a few kcal/mol, when alkylated phosphines are employed. However, ΔG for this bimolecular reaction will remain substantially positive, and the equilibrium for the formation of **4a** will thus lie far toward

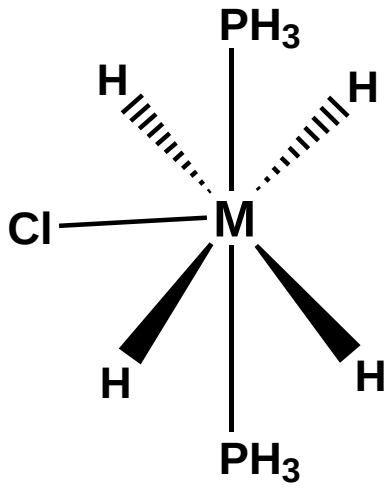

3

a, M=Rh; **b**, M=Ir

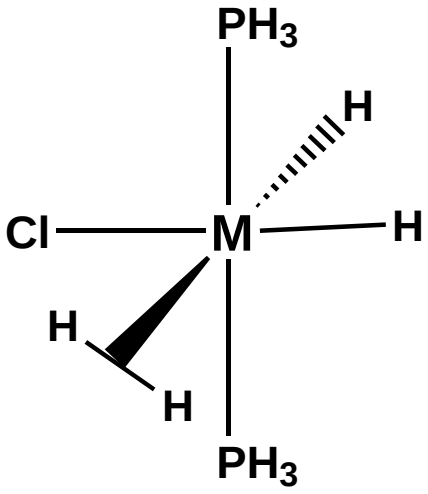

4

a, M=Rh; **b**, M=Ir

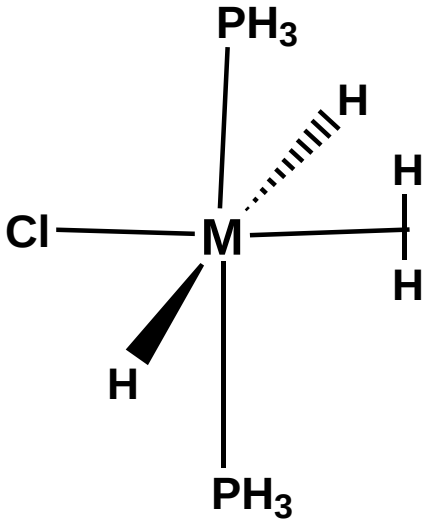

5

a, M=Rh; **b**, M=Ir

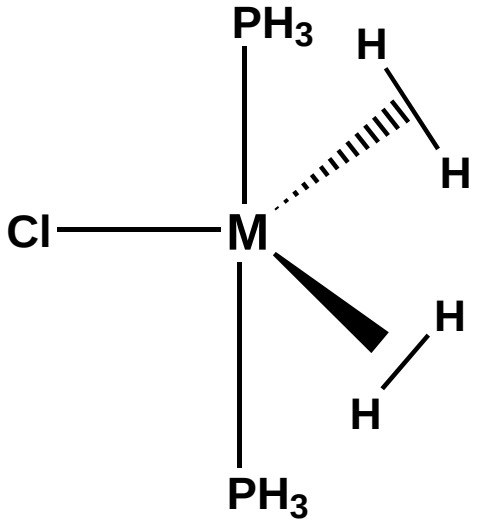

6

a, M=Rh; **b**, M=Ir

Figure 4.8: Isomers of the seven-coordinate M(V) complex.

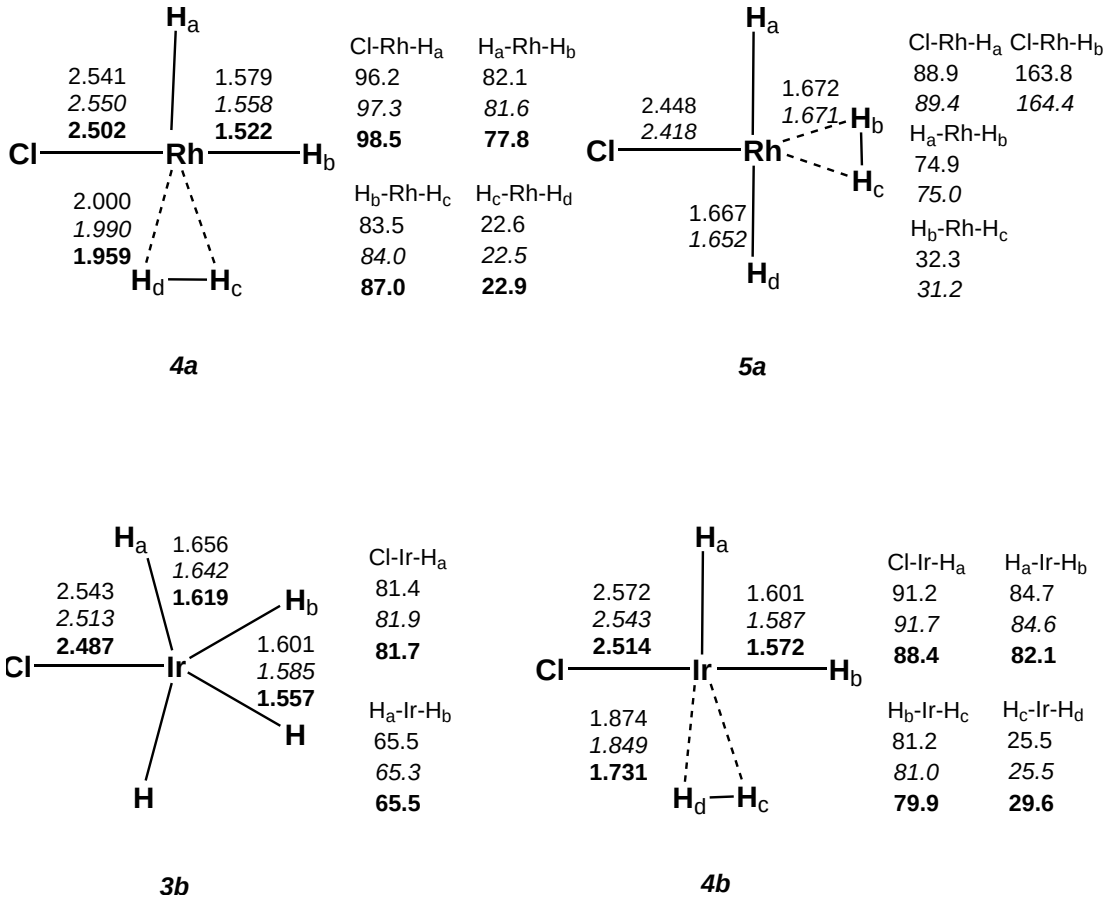

Figure 4.9: Optimized geometries of $H_4M(PH_3)_2Cl$ isomers, M = Rh and Ir. Bond lengths in $\mathring{A}$, angles in degrees. Phosphine groups omitted for clarity. BLYP: regular font; B3LYP: *italics*; MP2: **bold**.

the reactants (**trans-2a**, H_2) under normal experimental conditions.

When M = Ir, we locate the classical, four hydride isomer, **3b**, and the non-classical cis isomer, **4b**, as minima with all computational methods. With the singular exception of MP2, the methods agree that **4b** is slightly more stable than **3b**. The **3b-4b** enthalpy difference (Table 4.4) is more than 5 kcal/mol with the DFT methods, but decreases to 2 kcal/mol or less at the highly correlated levels (MP4(SDTQ): 1.3 kcal/mol; CCSD(T): 2.0 kcal/mol). Lin and Hall found that the use of PH_3 rather than PMe_3 in calculations tended to favor the non-classical isomers [103], but there are no indications of the non-classical trans

Table 4.4: Relative Enthalpies (ΔH, kcal/mol) of $H_4M(PH_3)_2Cl$ Species

Species	BLYP	B3LYP	MP2	MP4(SDTQ)	CCSD(T)
M = Rh					
4a	0.0	0.0	0.0		
5a	21.0	22.3	[a]		
M = Ir					
4b	0.0	0.0	0.0	0.0	0.0
3b	5.6	7.3	-1.3	1.3	2.0

[a] Not a stationary point on the MP2 surface.

isomer **5b** (or of **6**) when the computational method used for geometry optimization includes electron correlation [104]. Relativistic effects (destabilization of the 5d orbitals) should preferentially favor classical isomers [105], and, indeed, we could not locate the classical tetrahydride when M = Rh (see above). There is NMR evidence pointing to a non-classical structure for $H_4Ir(P^iPr_3)_2Cl$ [106], in accord with the computational results (Table 4.4). According to the MO based correlation methods, the seven-coordinate species **4b** is moderately bound with respect to *trans*-**2b** and H_2 (ΔH = -8.6 kcal/mol (MP2), -8.1 kcal/mol (MP4), -6.8 kcal/mol at CCSD(T)). However, the formation reaction is predicted to be essentially thermoneutral at the DFT levels (ΔH = 0.1 kcal/mol (BLYP), -1.9 kcal/mol (B3LYP)).

The transition state leading to the non-classical cis-isomer (**7**, Fig. 4.10) finds H_2 at a large distance (2.6 Å) from the metal center and only slightly activated (H-H $\sim$ 0.75 Å). The transition state leading to **4** is only 1-3 kcal/mol above the reactants for both M = Rh and Ir. We have been unable to find a transition state, which leads directly to the classical isomer **3b** or to the trans non-classical isomer **5a** from the separated reactants. However, **3b** should be readily formed by intramolecular rearrangement. Transition state **8b** (Fig. 4.10), which connects **4b** and **3b** is located only 2.8 kcal/mol (CCSD(T)) above **4b**. The classical tetrahydride **3b** forms only a shallow minimum, since **3b** and **8b** are computed to

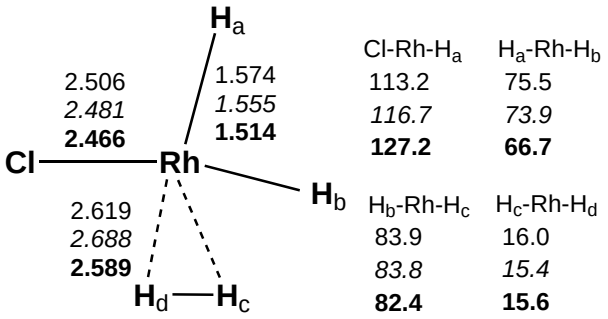

7a

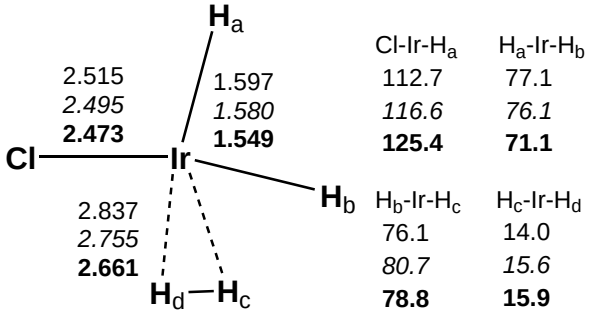

7b

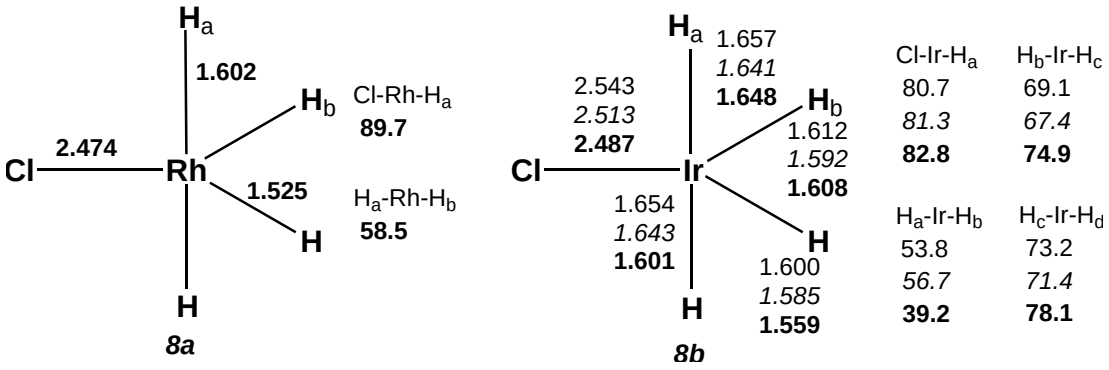

8a ***8b***

Figure 4.10: Optimized geometries for transition states **7** and **8**. Bond lengths in $\AA$, angles in degrees. BLYP: regular font; B3LYP: *italics*; MP2: **bold**.

be very close energetically (0.3 kcal/mol at CCSD(T)) and structurally (cf. Figs. 4.9 and 4.10) by all methods. On the MP2 surface for M = Rh, the four hydride species **8a** represents the transition state for the degenerate interconversion of the two equivalent non-classical cis-isomers **4a**; **8a** is 13.0 kcal/mol higher in enthalpy than **4a**.

4.5 Conclusions

All three computational methods used here for geometry optimizations (BLYP, B3LYP, and MP2) produce comparable structures for all the isomers. Bond lengths from MP2 are shorter than those obtained from DFT (Figs. 4.2, 4.5, 4.9, 4.10); bond lengths from B3LYP tend to be slightly shorter than those from BLYP, probably reflecting the small admixture of Hartree-Fock exchange present in the B3 functional. There is also general agreement among the methods regarding the relative energies of isomers (Tables 4.1 and 4.3). In particular, for $M(PH_3)_2Cl$ (M = Rh and Ir) the singlet T_{PH_3} structure is clearly the preferred isomer. It is noteworthy that the enthalpy differences among the M(I) and M(III) isomers predicted by the B3LYP method are very similar to those predicted by the far more elaborate CCSD(T) method [107]. Large differences appear in computed reaction enthalpies for dihydrogen addition with the MO-based methods (MPn, CCSD(T)) predicting considerably higher exothermicities, which translate into larger M-H bond energies. The MO-based results appear to be closer to the available (limited) experimental data, and the DFT methods thus underestimate the M-H bonding energies, although they do produce the better results for the intrinsic H-H bond enthalpy. The apparent ability of the MPn/CCSD methods to form stronger M-H bonds is on display in the Ir(V) complexes, where a very small enthalpy difference is predicted between classical and non-classical isomers.

The structural and energetic influences exerted by bulky phosphines continue

to be of interest. Unfortunately, the dramatic scaling of MPn/CCSD(T) calculations with molecular size makes it impossible to perform these highly accurate calculations on large systems [108]. DFT calculations scale less unfavorably with molecular size and would seem to be the method of choice for further investigations of such "substituent" effects.

Chapter 5

Computational Determination of the Electronic Spectra of Anticancer Drugs

Significant advances have been made in site-specific drug delivery and time release polymeric systems.[123] Amongst these advances, drug delivery systems for use in anti-cancer treatment are perhaps the most significant.[124] A number of these anti-cancer drugs are strongly fluorescent and therefore may be traced continually during the drug delivery and degradation process.

The study presented in the previous chapter involved application of ground state theories. Here we study electronic excitations within molecules, an application of time-dependent density functional methods. I describe on-going computational studies to determine the spectra of two drugs: 20-S-camptothecin (CPT) and Methotrexate (MTX). While their spectra can be determined experimentally without much difficulty, it is important to establish reliability in predicting excitations within these compounds. For drugs that are harmful upon exposure, one can easily see how it is useful to be able to predict their properties without having to actually handle the drugs. All calculations in this chapter were done using the GAUSSIAN03 code [16].

5.1 20-S-Camptothecin

The ability of CPT (Fig. 5.1) to inhibit tumor growth has long been known [125]. However, a major problem is that the potent anti-tumor properties of CPT and

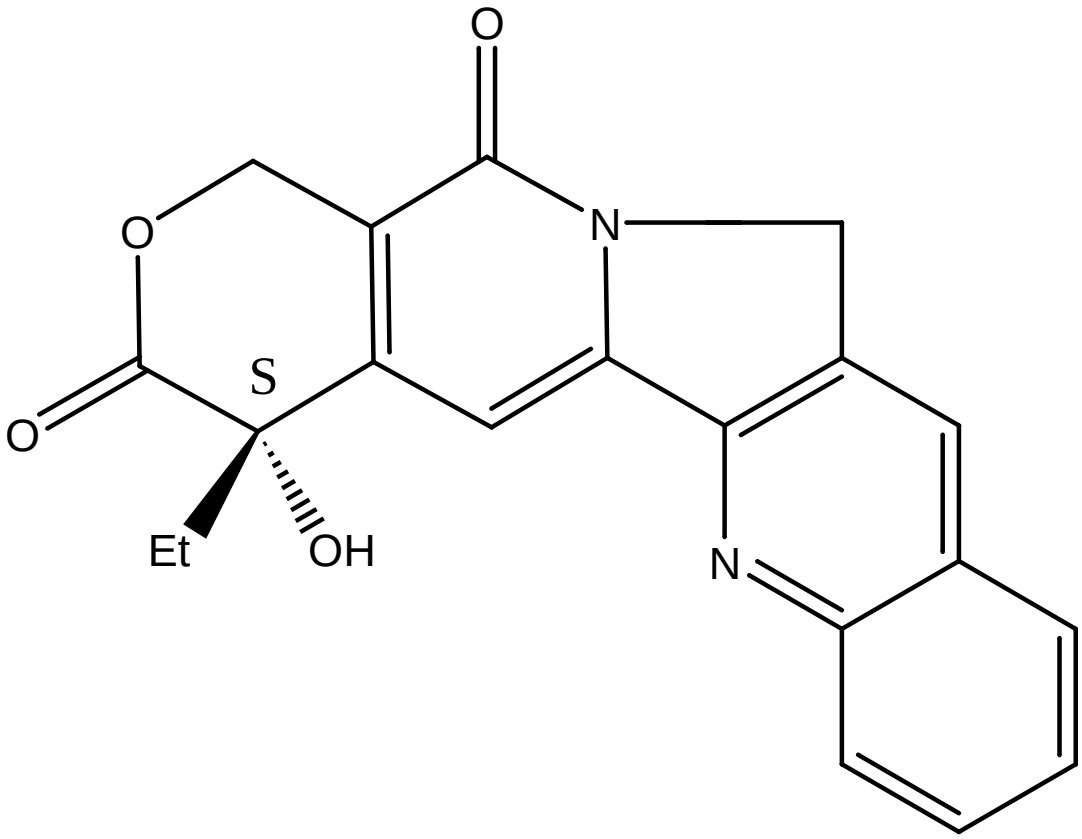

Figure 5.1: Lactone form of 20-S-camptothecin. This is the active tumor-inhibiting form of the drug.

its derivatives are lost and the drug becomes toxic upon opening of the α-hydroxy-lactone ring to form a carboxylate (Fig. 5.2). This lactone hydrolysis reaction occurs in non-acidic media including under physiological conditions. Therefore, CPT has not been extensively used in clinical applications. Interest in a number of CPT derivatives [126, 127] and their abilities to hinder tumor growth in humans was revived in the late 1980s [128, 129, 130]. CPT's fluorescent properties lend it to monitoring as it is absorbed in the body and as it interacts with DNA and other molecules.

Optimization of the ground state of CPT was performed at the B3LYP/6-31G* level. We performed time-dependent DFT calculations on ground and CIS

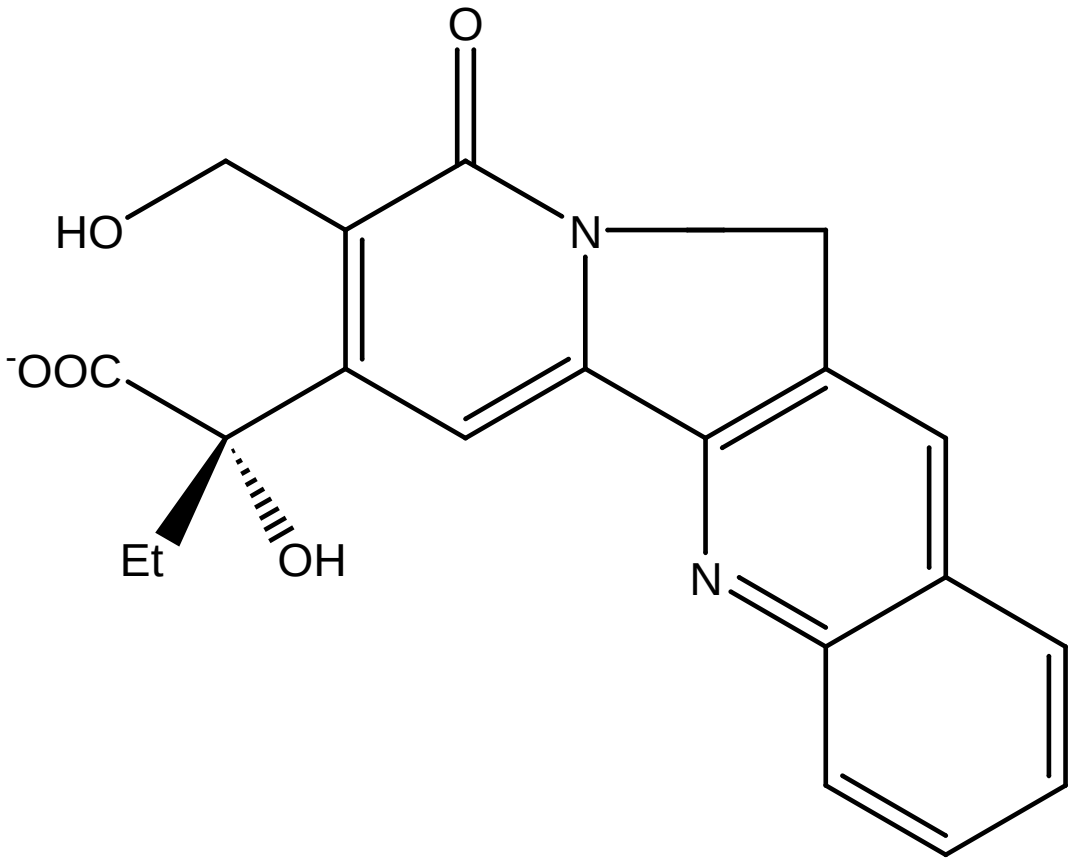

Figure 5.2: Carboxylate of 20-S-camptothecin formed by α-hydroxy-lactone ring opening under physiological conditions. This form of CPT is inactive and toxic.

Table 5.1: TD B3LYP predicted wavelengths (nm) of the first ten excitations of the ground-state optimized 20-S-CPT molecule in various solvents.

Excitation	vacuum *<1	heptane *1.92	THF *7.58	ethanol *24.6	acetonitrile *36.6	DMSO *46.7	water *78.4
1	376.9	372.7	364.4	361.9	361.4	362.5	361.0
2	317.9	321.4	325.3	326.2	326.3	326.8	326.3
3	304.1	301.1	296.1	294.7	294.5	294.6	294.0
4	303.2	299.7	296.0	294.5	294.2	294.5	293.9
5	300.0	293.7	285.9	285.6	285.5	285.7	285.4
6	285.3	286.1	284.2	281.5	281.1	281.2	280.4
7	275.9	268.3	261.5	260.1	259.9	259.8	259.8
8	257.9	256.6	255.5	255.3	255.2	255.5	255.2
9	256.5	250.7	252.3	252.3	252.6	253.1	252.6
10	247.6	250.0	243.2	241.3	241.2	241.3	241.2

*value of the dielectric constant, ϵ.

optimized excited state geometries. To simulate solvent effects and environments, calculations were done using the TD B3LYP method at various values of the dielectric constant, ϵ, ranging from < 1 to $\sim$80.

Tables 5.1 and 5.2 summarize the results of our CPT calculations. We study solvent effects on excitations in the molecule by varying the dielectric constant, ϵ, which increases from left to right in the tables. The general trend observed is that the transition energy increases with increasing dielectric constant; the only exception being in the presence of the DMSO solvent where there is a slight decrease in absorption energy relative to acetonitrile. Tables 5.3 and 5.4 list the wavelengths and oscillator strengths of the first ten excitations of CPT in water at the ground and excited state geometries, respectively.

Experimental studies of the absorption and fluorescence spectra of CPT and its derivatives are given in Reference [131]. The measured maximum excitation wavelength, λ_{abs}, of CPT in aqueous solution at a pH of 5.0 or 7.3 is 370 nm. Our DFT predicted absorption wavelength is 361.0 nm for the optimized ground state geometry (Tables 5.1 and 5.3). This is a remarkably accurate prediction,

Table 5.2: TD B3LYP predicted wavelengths (nm) of the first ten excitations of the CIS optimized 20-S-CPT molecule in various solvents.

Excitation	vacuum *<1	heptane *1.92	THF *7.58	ethanol *24.6	acetonitrile *36.6	DMSO *46.7	water *78.4
1	404.9	405.0	397.0	394.1	393.5	395.6	393.1
2	330.0	333.0	336.5	337.5	337.6	337.9	337.6
3	319.9	312.3	309.0	307.7	307.5	307.6	306.9
4	313.3	310.2	302.5	300.8	300.5	300.8	300.2
5	310.0	307.9	299.7	296.7	296.3	296.3	295.4
6	292.9	290.6	290.4	290.2	290.1	290.4	290.0
7	288.4	283.8	276.2	273.8	273.5	273.9	273.3
8	262.4	260.7	258.9	258.5	258.4	258.5	258.3
9	254.2	250.3	250.2	250.1	250.0	250.5	249.9
10	249.3	246.2	240.4	240.1	240.2	240.2	240.2

*value of the dielectric constant, ϵ.

Table 5.3: TD B3LYP predicted wavelengths (nm) and oscillator strengths of the first ten excitations in water at the CPT ground state geometry.

Excited state	Wavelength (nm)	Oscillator strength
1	361.0	0.4778
2	326.3	0.0341
3	294.0	0.0807
4	293.9	0.0143
5	285.4	0.1184
6	280.4	0.0002
7	259.8	0.0051
8	255.2	0.1176
9	252.6	0.3194
10	241.2	0.0249

Table 5.4: TD B3LYP predicted wavelengths (nm) and oscillator strengths of the first ten excitations in water at the CIS optimized CPT excited state geometry.

Excited state	Wavelength (nm)	Oscillator strength
1	393.1	0.5981
2	337.6	0.0481
3	306.9	0.0012
4	300.2	0.0480
5	295.4	0.0123
6	290.0	0.1806
7	273.3	0.0019
8	258.3	0.0334
9	249.9	0.3571
10	240.2	0.0188

Table 5.5: TD B3LYP computed Stokes shift (cm^{-1}) of CPT in the gas phase and various solvents.

vacuum	heptane	THF	ethanol	acetonitrile	DMSO	water	Expt.[a]
<1	*1.92	*7.58	*24.6	*36.6	*46.7	*78.4	
1835	2140	2253	2258	2257	2308	2262	3879

* value of the dielectric constant, ϵ.

[a] experimentally determined value in water[131].

especially given the limited basis set applied, and is an excellent illustration of the power and predictability of DFT. The emission wavelength, λ_{em}, on the other hand, is grossly underestimated with a TD B3LYP predicted value of 393.1 nm and an experimentally observed $\lambda_{em} = 432$ nm.

Fluorescent emissions correspond to longer wavelengths than those typically observed in absorption. This shift to longer wavelengths is called the Stokes shift and is computed by taking the difference between the fluorescence and absorption wavelengths, $\frac{1}{\lambda_{abs}} - \frac{1}{\lambda_{em}}$. Table 5.5 shows the TD B3LYP computed Stokes shift of the CPT molecule in various environments.

5.2 Methotrexate

Methotrexate (MTX) is a popular anti-cancer/anti-rheumatic drug. It blocks an enzyme required for cell life, thereby killing cancer (as well as healthy) cells.

My calculations on MTX have not been as successful as those on CPT because the number of geometrical degrees of freedom in MTX is significantly greater than that of the more rigid, planar CPT (compare Figs. 5.1 and 5.3). This makes optimization of MTX very difficult. Therefore, at this time, I am only able to report results for the excited states of MTX as predicted by time-dependent B3LYP/6-31G* calculations on the ground state optimized geometry in vacuum. The wavelengths and oscillator strengths of the first ten excitations are listed in table 5.6.

5.3 Future Directions

One study not considered here is the spectrum of the ring-opened carboxylate form of the CPT molecule as well as the CPT derivatives known to be cancer inhibitors. The thermodynamics and kinetics of the ring-opening process would also be interesting to consider. Calculations for determination of the fluorescence

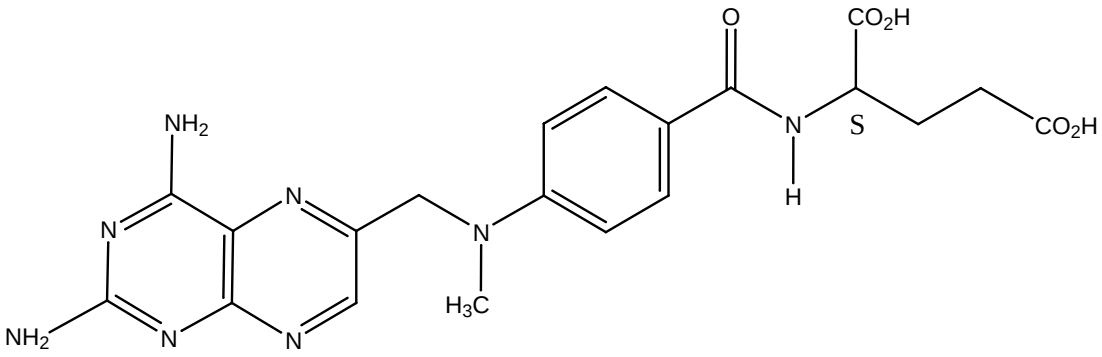

Figure 5.3: Structure of the Methotrexate molecule.

Table 5.6: TD B3LYP predicted wavelengths (nm) and oscillator strengths of the first ten excitations in the gas phase at the MTX ground state geometry.

Excited state	Wavelength (nm)	Oscillator strength
1	353.95	0.1178
2	368.87	0.0021
3	421.86	0.0001
4	292.77	0.0019
5	288.04	0.0028
6	284.20	0.0022
7	281.74	0.0172
8	278.72	0.0028
9	273.12	0.0644
10	271.98	0.5117

spectrum of MTX remains to be completed and solvent effects explored.

References

[1] W. Koch and M.C. Holthausen, *A Chemist's Guide to Density Functional Theory*, (New York, Wiley-VCH, 2000).

[2] P.Hohenberg & W. Kohn, Phys. Rev. B **136**, 864 (1964).

[3] W. Kohn and L.J. Sham, Phys. Rev. **140**, A 1133 (1965).

[4] W. Kohn, Rev. Mod. Phys. **71**, 1253 (1999).

[5] J. Pople in *Nobel Lectures, Chemistry 1996-2000*, ed. I. Grenthe, World Scientific Publishing Co., Singapore (2003).

[6] C.J.H. Jacobsen, S. Dahl, B.S. Clausen, S. Bahn, A. Logadottir, and J.K. Nørskov,

[7] C.J. Cramer, *Essentials of computational chemistry: theories and models*, ed. John Wiley & Sons, Inc., Chichester, England (2002).

[8] D.R. Hartree, Proc. Cambridge Phil. Soc. **24**, 89, 111, 426 (1928).

[9] C.C.J. Roothaan, Rev. Mod. Phys. **23**, 69 (1951).

[10] A. Szabo and N.S. Ostlund, *Modern Quantum Chemistry*, (New York, Macmillan, 1982).

[11] M. Head-Gordon, J.A. Pople, and M. Frisch, J. Chem. Phys. Lett. **153**, 503 (1988).

[12] R. Krishnan, M.J. Frisch, and J.A. Pople, J. Chem. Phys. **72**, 4244 (1980).

[13] J.A. Pople, M. Head-Gordon, and K. Raghavachari, J. Chem. Phys. **87**, 5968 (1987).

[14] G.D. Purvis and R.J. Bartlett, J. Chem. Phys. **76**, 1910 (1982).

[15] Gaussian 98 (Revision A.5), MJ Frisch, GW Trucks, HB Schlegel, GE Scuseria, MA Robb, JR Cheeseman, VG Zakrzewski, JA Montgomery, RE Stratmann, JC Burant, S Dapprich, JM Millam, AD Daniels, KN Kudin, MC Strain, O Farkas, J Tomasi, V Barone, M Cossi, R Cammi, B Mennucci, C Pomelli, C Adamo, S Clifford, J Ochterski, GA Petersson, PY Ayala, Q Cui, K Morokuma, DK Mailick, AD Rabuck, K Raghavachari, JB Foresman, J

Cioslowski, JV Ortiz, BB Stefanov, G Liu, A Liashenko, P Piskorz, I Komaromi, R Gomperts, RL Martin, DJ Fox, T Keith, MA Al-Laham, CY Peng, A Nanayakkara, C Gonzalez, M Challacombe, PMW Gill, BG Johnson, W Chen, MW Wong, JL Andres, M Head-Gordon, ES Replogle, JA Pople. Pittsburgh, PA: Gaussian Inc., 1998.

[16] Gaussian 03, Revision B.02, M. J. Frisch, G. W. Trucks, H. B. Schlegel, G. E. Scuseria, M. A. Robb, J. R. Cheeseman, J. A. Montgomery, Jr., T. Vreven, K. N. Kudin, J. C. Burant, J. M. Millam, S. S. Iyengar, J. Tomasi, V. Barone, B. Mennucci, M. Cossi, G. Scalmani, N. Rega, G. A. Petersson, H. Nakatsuji, M. Hada, M. Ehara, K. Toyota, R. Fukuda, J. Hasegawa, M. Ishida, T. Nakajima, Y. Honda, O. Kitao, H. Nakai, M. Klene, X. Li, J. E. Knox, H. P. Hratchian, J. B. Cross, C. Adamo, J. Jaramillo, R. Gomperts, R. E. Stratmann, O. Yazyev, A. J. Austin, R. Cammi, C. Pomelli, J. W. Ochterski, P. Y. Ayala, K. Morokuma, G. A. Voth, P. Salvador, J. J. Dannenberg, V. G. Zakrzewski, S. Dapprich, A. D. Daniels, M. C. Strain, O. Farkas, D. K. Malick, A. D. Rabuck, K. Raghavachari, J. B. Foresman, J. V. Ortiz, Q. Cui, A. G. Baboul, S. Clifford, J. Cioslowski, B. B. Stefanov, G. Liu, A. Liashenko, P. Piskorz, I. Komaromi, R. L. Martin, D. J. Fox, T. Keith, M. A. Al-Laham, C. Y. Peng, A. Nanayakkara, M. Challacombe, P. M. W. Gill, B. Johnson, W. Chen, M. W. Wong, C. Gonzalez, and J. A. Pople, Gaussian, Inc., Pittsburgh PA, 2003.

[17] J. P. Perdew and Y. Wang, Phys. Rev. B 45, 13244-13249 (1992).

[18] J.P. Perdew, K. Burke, and M. Ernzerhof, Phys. Rev. Lett. **77**, 3865 (1996); **78**, 1396 (1997) (E).

[19] K. Burke, M. Petersilka, and E.K.U. Gross in *Recent advances in density functional methods*, eds. V. Barone, A. Bencini, and P. Fantucci, World Scientific (2002), p. 67.

[20] A.D. Becke, J. Chem. Phys. **98**, 1372 (1993).

[21] A.D. Becke, J. Chem. Phys. **98**, 5648 (1993).

[22] M. Levy and J.P. Perdew, Phys. Rev. A **32**, 2010 (1985).

[23] I.N. Levine, *Quantum Chemistry*, (Boston, Allyn and Bacon, 1974).

[24] J.P. Perdew and S. Kurth, in *Density functionals: Theory and applications*, ed. D. Joubert (Springer, Berlin, 1998).

[25] R.J. Magyar, T.K. Whittingham, and K. Burke, Phys Rev A **66**, 022105 (2002).

[26] U. von Barth and L. Hedin, J. Phys. C **5**, 1629 (1972).

[27] Rajagopal, A.K, Calloway, Phys. Rev. B **7**, 1912-1919 (1973)

[28] D.C. Langreth and J.P. Perdew, Solid State Commun. **17**, 1425 (1975).

[29] O. Gunnarsson and B.I. Lundqvist, Phys. Rev. B **13**, 4274 (1976).

[30] K. Burke, M. Ernzerhof, and J.P. Perdew, Chem. Phys. Lett. **265**, 115 (1997).

[31] J.P. Perdew, M. Ernzerhof, and K. Burke, J. Chem. Phys. **105**, 9982 (1996).

[32] Y.A. Wang, Phys. Rev. A, **56**, 1646 (1997).

[33] K. Burke in *Electronic Density Functional Theory: Recent Progress and New Directions*, eds. J.F. Dobson, G. Vignale, and M.P. Das (Plenum, NY, 1997), page 19.

[34] A. D. Becke, Phys. Rev. A 38, 3098-3100 (1988).

[35] C. Lee, W. Yang, and R.G. Parr, Phys. Rev. B **37**, 785 (1988).

[36] J. P. Perdew and A. Zunger, Phys. Rev. B **23**, 5048 (1981).

[37] C.J. Umrigar and X. Gonze, Pys. Rev. A, **50**, 3827 (1994).

[38] D. Frydel, W. Terilla, and K. Burke, J. Chem. Phys. **112**, 5292 (2000).

[39] E. Davidson, S. Hagstrom, S. Chakravorty, V. Umar, and F. Fischer, Pys. Rev. A, **44**, 7071 (1991).

[40] R.C. Morrison, and Q. Zhao, Phys. Rev. A **51**, 1980 (1995).

[41] K. Burke, J.P. Perdew, and M. Ernzerhof, in *Electronic Density Functional Theory: Recent Progress and New Directions*, eds. J.F. Dobson, G. Vignale, and M.P. Das (Plenum, NY, 1997), page 57.

[42] A. Görling and M. Levy, Phys. Rev. A **50**, 196 (1994).

[43] P. Süle, Chem. Phys. Lett. **259**, 69 (1996).

[44] K. Burke, F.G. Cruz, and K.C. Lam, J. Chem. Phys. 109, 8161 (1998).

[45] A. Görling and M. Levy, Phys. Rev. A **45**, 1509 (1992).

[46] K. Burke, J. P. Perdew, and M. Levy, in *Modern Density Functional Theory: A Tool for Chemistry*, edited by J. M. Seminario and P. Politzer (Elsevier, Amsterdam, 1995).

[47] R.G. Parr and W. Yang (Oxford, New York, 1989).

[48] Y.A. Wang, Phys. Rev. A **56**, 1646 (1997).

[49] E.R. Davidson, S.A. Hagstrom, S.J. Chakravorty, V. Meiser Umar, and C. Froese Fischer, Phys. Rev. A **44**, 7071 (1991).

[50] S.J. Chakravorty, S.R. Gwaltney, E.R. Davidson, F.A. Parpia, and C. Froese Fischer, Phys. Rev. A **47**, 3649 (1993).

[51] E. Engel and R.M. Dreizler, J. Comput. Chem. **20**, 31 (1999).

[52] C.J. Huang and C.J. Umrigar, Phys. Rev. A **56**, 290 (1997).

[53] M. Levy, Phys. Rev. A **43**, 4637 (1991).

[54] J. Harris and R.O. Jones, J. Phys. F **4**, 1170 (1974).

[55] D.C. Langreth and J.P. Perdew, Phys. Rev. B **15**, 2884 (1977).

[56] A. Görling and M. Levy, Phys. Rev. B **47**, 105 (1993).

[57] E.R. Davidson, Int. J. Quant. Chem. **69**, 241 (1998).

[58] A. Görling and M. Ernzerhof, Phys. Rev. A **51**, 4501 (1995x).

[59] E.P. Ivanova and U.I. Safronova, J. Phys. B: Atom. Molec. Phys. **8**, 1591 (1975).

[60] S. Ivanov and M. Levy, J. Phys. Chem. A **102**, 3151 (1998).

[61] C. Filippi, X. Gonze, and C.J. Umrigar, in *Recent Developments and Applications of Density Functional Theory*, ed. J.M. Seminario (Elsevier, Amsterdam, 1996).

[62] E. Clementi and C. Roetti, At. Data Nucl. Data Tables **14**, 177 (1974).

[63] O. Jitrik and C.F. Bunge, Phys. Rev. A **43**, 5804 (1991).

[64] Q. Zhao and R.G. Parr, Phys. Rev. A **46**, 2337 (1992).

[65] Q. Zhao and R.G. Parr, J. Chem. Phys. **98**, 543 (1992).

[66] Q. Zhao, R.C. Morrison, and R.G. Parr, Phys. Rev. A **50**, 2138 (1994).

[67] V.N. Staroverov, G.E. Scuseria, J.P. Perdew, J. Tao, and E.R. Davidson, submitted to Phys. Rev. A (2004).

[68] Y. Wang and J.P.Perdew, Phys. Rev. B **43**, 8911 (1991).

[69] S. Ivanov, K. Burke, and M. Levy, J. Chem. Phys. **110**, 10262 (1999).

[70] A.A. Jarzecki and E.R. Davidson, Mol. Phys. **98**, 1089 (2000).

[71] A. Facco Bonetti, E. Engel, R.N. Schmid, and R.M. Dreizler, Phys. Rev. Lett. **86**, 2241 (2001).

[72] S. Niu and M.B. Hall, J. Am. Chem. Soc. **121**, 3992 (1999).

[73] K. Krogh-Jespersen, M. Czerw, and A.S. Goldman, J. Chem. Info. Comput. Sci. **41**, 56 (2001).

[74] M. Czerw, T.K. Whittingham, and K. Krogh-Jespersen in *Computational Organometallic Chemistry*, pp. 323-343, ed. T.R. Cundari, Marcel Dekker, Inc. (2001).

[75] W.J. Hehre, L. Radom, J.A. Pople, and PvR Schleyer, *Ab Initio Molecular Orbital Theory*, New York: Wiley-Interscience, (1986).

[76] P.J. Hay and W.R. Wadt, J. Chem. Phys. **82**, 270 (1985).

[77] T.H. Dunning and P.J. Hay, *Modern Theoretical Chemistry; HF Schaefer III*, Ed. New York: Plenum, pp. 1-28 (1976).

[78] R. Krishnan, J.S. Binkley, R. Seeger, and J.A. Pople, J. Chem. Phys. **72**, 650 (1980).

[79] J.S. Binkley, J.A. Pople, and W.J. Hehre, J. Am. Chem. Soc. **102**, 939 (1980).

[80] W.J. Hehre, R.F. Stewart, and J.A. Pople, J. Chem. Phys. **51**, 2657 (1969).

[81] D.A. McQuarrie, *Statistical Thermodynamics*, New York: Harper and Row, (1973).

[82] T.A. Albright, J.K. Burdett, M.H. Whangbo, *Orbital Interactions in Chemistry*, Wiley-Interscience, (1985).

[83] J.F. Riehl, Y. Jean, O. Eisenstein, and M. Pelissier, Organometallics **11**, 729 (1992).

[84] P. Margl, T. Ziegler, and P.E. Bloechl, J. Am. Chem. Soc. **117**, 12625 (1995).

[85] M.D. Su and S.Y. Chu, J. Am. Chem. Soc. **119**, 10178 (1997).

[86] J.D. Atwood, *Inorganic and Organometallic Reaction Mechanisms*, Monterey: Brooks/Cole Publishing Co., (1985).

[87] T.R. Cundari, J. Am. Chem. Soc. **116**, 340 (1994).

[88] G.P. Rosini, F. Liu, K. Krogh-Jespersen, A.S. Goldman, C. Li, and S.P. Nolan, J. Am. Chem. Soc. **120**, 9256 (1998).

[89] K. Krogh-Jespersen, A.S. Goldman, *Transition State Modeling for Catalysis*, ACS Symposium Series No. 721, eds. D.G. Truhlar and K. Morokuma, pp. 151-162 (1998).

[90] P.E.M. Siegbahn, J. Am. Chem. Soc. **118**, 1487 (1996).

[91] C.J. van Wüllen, J. Comput. Chem. **18**, 1985 (1997).

[92] K. Wang, G.P. Rosini, S.P. Nolan, and A.S. Goldman, J. Am. Chem. Soc. **117**, 5082 (1995).

[93] W. Xu, G.P. Rosini, M. Gupta, C.M. Jensen, W.C. Kaska, K. Krogh-Jespersen, and A.S. Goldman, Chem. Commun. 2273 (1997).

[94] M. Gupta, C. Hagen, R.J. Flesher, W.C. Kaska, and C.M. Jensen, Chem. Comm. 2083 (1996).

[95] R.G. Pearson, Acc. Chem. Res. **4**, 152 (1971).

[96] G.S. Hammond, J. Am. Chem. Soc. **77**, 334 (1955).

[97] CRC Handbook of Chemistry and Physics. 71st ed. DR Lide. Ed. Boca Raton FL, CRC Press, (1990).

[98] F.A. Cotton and G. Wilkinson, *Advanced Inorganic Chemistry* 6th ed.; New York, John Wiley & Sons, (1999).

[99] G. Kubas, Acc. Chem. Res. **21**, 120 (1988).

[100] P.G. Jessop and R.J. Morris, Coord. Chem. Rev. **121**, 155 (1992).

[101] Z. Lin and M.B. Hall, Inorg. Chem. **31**, 4262 (1992).

[102] Z. Lin and M.B. Hall, J. Am. Chem. Soc. **114**, 6102 (1992).

[103] Z. Lin and M.B. Hall, J. Am. Chem. Soc. **114**, 2928 (1992).

[104] Structure **5b** is a minimum at the Hartree-Fock level, see reference [100].

[105] J. Li, R.M. Dickson, and T. Ziegler, J. Am. Chem. Soc. **117**, 11482 (1995).

[106] M. Mediati, G.N. Tachibana, and C.M. Jensen, Inorg. Chem. **29**, 3 (1990).

[107] R.K. Szilagyi and G. Frenking, Organometallics **16**, 4807 (1997).

[108] B.G. Johnson, P.M.W. Gill, and J.A. Pople, J. Chem. Phys. **97**, 7846 (1992).

[109] J. Burdeniuc, B. Jedlicka, and R.H. Crabtree, Chem. Ber/Recueil **130**, 145 (1997).

[110] K. Nomura and Y. Saito, Chem. Commun. **161**, (1988).

[111] T. Sakakura, T. Sodeyama, M. Tokunaga, and M. Tanaka, Chem Lett p. 263, (1988).

[112] J.B. Foresman and A. Frisch, *Exploring Chemistry with Electronic Structure Methods*, Pittsburgh, PA: Gaussian Inc., 1996.

[113] H.B. Schlegel, *Modern Electronic Structure Theory*, DR Yarkony. Ed. Singapore: World Scientific Publishing, pp. 459-500 (1994).

[114] N. Koga, K. Morokuma, J. Phys. Chem. **94**, 5454 (1990).

[115] C. Daniel, N. Koga, J. Han, X.Y. Fu, and K. Morokuma, J. Am. Chem. Soc. bf 110, 3773 (1988).

[116] N. Koga and K. Morokuma, J. Am. Chem. Soc. **115**, 6883 (1993).

[117] D.G. Musaev and K. Morokuma, J. Organomet. Chem. **504**, 93 (1995).

[118] M.R.A. Blomberg, P.E.M. Siegbahn, and M. Svensson, J. Am. Chem. Soc. **114**, 6095 (1992).

[119] Y.W. Yared, S.L. Miles, R. Bau, and C.A. Reed, J. Am. Chem. Soc. **99**, 7076 (1977).

[120] A. Dedieu and I. Hyla-Kryspin, J. Organomet. Chem. **220**, 115 (1981).

[121] M. Gupta, C. Hagen, R.J. Flesher, W.C. Kaska, and C.M. Jensen, Chem. Commun. 2083 (1996).

[122] W.H.E. Schwarz, E.M. van Wezenbeek, E.J. Baerends, and J.G. Snijders, J. Phys. B: At. Mol. Opt. Phys. **22**, 1515 (1989).

[123] K.E. Uhrich, S.M. Cannizzaro, R.S. Langer, and K.M. Shakesheff, Chem. Rev. **99**, 3181 (1999).

[124] D.L. Emerson, Pharma. Sci. Tech. Today **3**, 205 (2000).

[125] M.E. Wall, M.C. Wani, C.E. Cook, K.H. Palmer, A.T. McPhail, and G.A. Sims, J. Am. Chem. Soc. **88**, 3888 (1966).

[126] M.E. Wall, *Biochemie und Physiologie der Alkaloide*, eds. K. Mothes and K. Schreiber, Akademie Verlag, Berlin, pp. 77-87 (1969).

[127] M.E. Wall and M.C. Wani, *Natural products and drug development*, eds. P.K. Larsen and H.K. Christensen, Munksgaard, Copenhagen, pp. 253-266 (1984).

[128] M.C. Wani, A.W. Nicholas, G. Manikumar, and M.E. Wall, J. Med. Chem. **30**, 1774 (1987).

[129] M.C. Wani, A.W. Nicholas, G. Manikumar, and M.E. Wall, J. Med. Chem. **30**, 2317 (1987).

[130] B.C. Ginovanella, J.S. Stehlin, M.C. Wall, A.W. Nicholas, L.F. Liu, R. Silber, and M. Potmesil, Science **246**, 1046 (1989).

[131] I. Chourpa, J-M. Millot, G.D. Sockalingum, J-F. Riou, and M. Manfait, Biochimica et Biophysica Acta **1379**, 353 (1998).

[132] W. Kohn, Rev. Mod. Phys. **71**, 1253 (1999).

[133] J.P. Perdew, E.R. McMullen, & A. Zunger, Phys. Rev. A **23**, 2785 (1981).

[134] A.A. Jarzecki & E.R. Davidson, Phys. Rev. A **58**, 1902 (1998).

[135] T.K. Whittingham and K. Burke, in preparation.

[136] V. Yu. Irkhin and M.I. Katsnel'son, Usp. Fiz. Nauk **164**, 705 (1994) [Sov. Phys. Usp. **37**, 659 (1994)].

[137] W.E. Pickett, Phys. Rev. Lett. **77**, 3185 (1996).

[138] A.J. Cohen and N.C. Handy, Mol. Phys. **99**, 607 (2001).

[139] M. Levy, Phys. Rev. A **43**, 4637 (1991).

[140] Q. Zhao, M. Levy, and R. Parr, Phys. Rev. A, **47**, 918 (1993).

[141] M. Levy and A. Görling, Int. J. Quant. Chem. **56**, 385 (1995).

[142] F.G. Cruz, K.C. Lam, and K. Burke, J. Phys. Chem. A. 102, 4911 (1998).

[143] K. Capelle and G. Vignale, Phys. Rev. Lett. 86, 5546-5549 (2001).

[144] B.G. Johnson, P.M.W.Gill, J.A.Pople, J. Chem. Phys. **98**, 5612 (1993).

[145] S. Matar and Alexander Mavromaras. J. Solid State Chem. **149**, 449 (2000).

[146] Y. Wang and J.P.Perdew, Phys. Rev. B **43**, 8911 (1991).

[147] Q. Zhao and R.G. Parr, Phys. Rev. A **46**, 2337 (1992).

[148] A. Görling and M. Levy, Phys. Rev. B **47**, 105 (1993).

[149] Q. Zhao, R.C. Morrison, and R.G. Parr, Phys. Rev. A **50**, 2138 (1994).

[150] C. Filippi, X. Gonze, and C.J. Umrigar, in *Recent Developments and Applications of Density Functional Theory*, ed. J.M. Seminario (Elsevier, Amsterdam, 1996).

[151] C.J. Huang and C.J. Umrigar, Phys. Rev. A **56**, 290 (1997).

[152] E.R. Davidson, Int. J. Quant. Chem. **69**, 241 (1998).

[153] S. Ivanov, K. Burke, and M. Levy, J. Chem. Phys. **110**, 10262 (1999).

[154] A.A. Jarzecki and E.R. Davidson, Mol. Phys. **98**, 1089 (2000).

[155] A. Facco Bonetti, E. Engel, R.N. Schmid, and R.M. Dreizler, Phys. Rev. Lett. **86**, 2241 (2001).

[156] G. H. Jóhannesson, T. Bligaard, A. V. Ruban, H. L. Skriver, K. W. Jacobsen, and J. K. Nørskov, Phys. Rev. Lett. **88**, 255506 (2002).

[157] R.O. Jones and O. Gunnarson, Rev. Mod. Phys. Vol **61**, 689 (1989).

[158] N. Argaman and G. Makov, Am. J. Phys. **68**, 69 (2000).

[159] F. Jensen, (Wiley and Sons, New York ,1999).

[160] V.A. Fock, Zeit.Phys.,1933, Bd. **81**, N 3, S. 195. JHCEcTcF, 1934, Vol. **4**, iss. 1, s. 1. Transactions GOI, Vol. **10**, iss. 92, s. 1.

[161] C. Møller and M. S. Plesset, Phys. Rev. **46**, 618 (1934).

[162] J.M. Thijssen, *Computational Physics*, (Cambridge University Press, New York, 1999).

[163] G. Onida, L. Reining, and A. Rubio, Rev. Mod. Phys. **74** 601 (2002).

[164] Robert G. Parr and Weitao Yang, *Density-Functional Theory of Atoms and Molecules*, (Oxford University Press, New York, 1989).

[165] J. C. Slater, Phys. Rev. **81**, 385 (1951); **82**, 538 (1951); **91**, 52 (1953).

[166] E. Wigner, Phys. Rev. 46, 1002 (1934) and E. Wigner, Trans. Faraday Soc. **34**, 678 (1938).

[167] D. Pines, Solid State Physics **1**,367 (1955).

[168] M. Gell-Mann and K.A. Brueckner, Phys. Rev. **106**, 364.

[169] Ulf von Barth, Chemica Scripta **26**,449 (1986).

[170] S. Kotochigova, Z.H. Levine, E.L. Shirley, M.D. Stiles, and C.W. Clark, Phys. Rev. A, **55**, 191 (1997). erratum Phys. Rev. A **56**, 5191 (1997).

[171] S. H. Vosko, L. Wilkes, and M. Nusair, Can. J. Phys. **58**, 1200 (1980).

[172] J. P. Perdew and Y. Wang, Phys. Rev. B **45**, 13244 (1992).

[173] D.C. Langreth and J.P. Perdew, Phys. Rev. B **21**, 5469 (1980).

[174] D.C. Langreth and M.J. Mehl, Phys. Rev. B **28**, 1809 (1983).

[175] J. P. Perdew and Y. Wang, Phys. Rev. B **46**, 12947 (1992); ibid. **56**, 7018 (1997) (E).

[176] M. Levy, Phys. Rev. A **26**, 1200 (1982).

[177] V. Barone, Chem. Phys. Lett. **226**, 392 (1994).

[178] E. Runge and E.K.U. Gross, Phys. Rev. Lett. **52**, 997 (1984).

[179] E.K.U.Gross, J.F.Dobson, and M.Petersilka, Topics in Current Chemisty, **181**, 81 (1996).

[180] Dage Sundholm, Chem. Phys. Lett. **302**, 480 (1999)

[181] F. Illas, R. M. Martin, J. Chem. Phys., **108**, 2519 (1997).

[182] B.L. Gyorffy, J.B. Staunton, and G.M. Stocks, in *Fluctuations in Density Functional Theory: Random metallic alloys and itinerant paramagnets*, eds. E.K.U. Gross and R.M. Dreizler, (Plenum, NY, 1995).

[183] N.T. Maitra, A. Wasserman, and K.Burke, in Electron Correlations and Materials Properties 2, ed. A. Gonis, N. Kioussis, M. Ciftan, (Kluwer/Plenum, 2003).

[184] Tuan, S (Editor), Sakurai, J.J, *Modern Quantum Mechanics (2nd Edition)*, (Addison-Wesley Pub Co. New York, 1994)

[185] G.L. Gilbert, Phys. Rev. B. **12** 2111 (1975).

[186] J.E. Harriman, Phys. Rev. A **24**, 680 (1981).

[187] G. Zumbach and K. Machke, Phys. Rev. A **28**, 544 (1983).

[188] E.R. Davidson, Chem. Phys. Lett. **246**, 209 (1995).

[189] *H. Englisch and R. Englisch*, Physica **121A**, 253 (1983).

[190] Q. Zhao and R.G. Parr, Phys. Rev. A **46**, 2337 (1992).

[191] Q. Zhao and R. Parr, Phys. Rev. A, **46**, 5320 (1992).

[192] S. Kurth, J. P. Perdew, Int. J. Quant. Chem. **77**, 814 (2000).

[193] John P. Perdew and Karla Schmidt, in *Density Functional Theory and Its Applications to Materials*, edited by V.E. Van Doren, K. Van Alseoy, and P. Geerlings (American Institute of Physics, 2001).

[194] M. Ernzerhof, K. Burke, and J.P. Perdew, in *Recent developments and applications in density functional theory*, ed. J.M. Seminario (Elsevier, Amsterdam, 1996).

[195] M. Ernzerhof, J.P. Perdew, and K. Burke, in *Density Functional Theory*, ed. R. Nalewajski, Spinger-Verlag, Berlin, 1996.

[196] J.P. Perdew, Phys. Rev. Lett. **55**, 1665 (1985); **55**, 2370 (1985) (E).

[197] J.P. Perdew, S. Kurth, A. Zupan, P. Blaha, Phys. Rev. Lett. **82**, 2544 (1999); **82**, 5179 (1999) (E).

[198] J. Tao, J.P. Perdew, V.N. Staroverov, and G.E. Scuseria, Phys. Rev. Lett.**91**, 146401 (2003).

[199] R. Neumann, R.H. Nobes, N.C. Handy, Mol. Phys. **87**, 1 (1996).

[200] S. Kümmel and J.P. Perdew, PRL **90**, 043004-1 (2003).

[201] J. P. Perdew, Chem. Phys. Lett. **64**, 127 (1979).

[202] M. Ernzerhof, Chem. Phys. Lett. **263**, 499 (1996).

[203] M.A. Buijse and E.J. Baerends, in *Density Functional Theory of Molecules, Clusters, and Solids*, ed. D.E. Ellis (Kluwer Academic Publishers, Amsterdam, 1995).

[204] J.P. Perdew, K. Burke, and Y. Wang, Phys. Rev. B **54**, 16533 (1996); **57**, 14999 (1998) (E).

[205] M. Levy, in *Density Functional Theory*, eds. R. Dreizler and E. K. U. Gross, NATO ASI Series (Plenum, New York, 1995).

[206] R. M. Dreizler and E. K. U. Gross, *Density-Functional Theory, An Approach to the Quantum Many-Body Problem* (Springer, Berlin Heidelberg, 1990).

[207] N.T. Maitra, F. Zhang, R.J. Cave and K. Burke, submitted to Phys. Rev. Lett. (2003).

[208] Q. Zhao, M. Levy, and R. Parr, Phys. Rev. A, **47**, 918 (1993).

[209] Z. Qian and V. Sahni, Phys. Rev. A **57**, 2527 (1998).

[210] C. Adamo and V. Barone, J. Chem. Phys. **110**, 6158 (1999).

[211] M.Seidl, J. Perdew, and S. Kurth, Phys. Rev. A **62**, 012502 (2000).

[212] K. Burke, J.P. Perdew, and M. Levy, Phys. Rev. A **53**, R2915 (1996).

[213] R.J. Magyar, W. Terilla, and K. Burke, J. Chem. Phys. **119**, 696 (2003).

[214] S. Kais, D.R. Herschbach, N.C. Handy, C.W. Murray, and G.J. Laming, J. Chem. Phys. **99**, 417 (1993).

[215] A. Görling and M. Levy, Phys. Rev. B **47**, 13105 (1993).

[216] A. Görling and M. Levy, Int. J. Quant. Chem. **29**, 93 (1995).

[217] J. Perdew, S. Kurth, and M. Seidl, International Journal of Modern Physics B, Vol. **15**, 1672 (2001).

[218] K. Burke, J. Perdew, and M. Ernzerhof, J. Chem. Phys. **109**, 3760 (1998).

[219] A. Savin, C. J. Umrigar, X. Gonze, Chem. Phys. Lett. **288**, 391 (1998).

[220] H. Appel, E.K.U. Gross, and K. Burke, Phys. Rev. Lett. **90**, 043005 (2003).

[221] C. J. Umrigar and X. Gonze, in *H*igh Performance Computing and its Application to the Physical Sciences, ed. D. A. Browne *et* al., Proceedings of the Mardi Gras '93 Conference (World Scientific, Singapore, 1993).

[222] Q. Zhao, R. C. Morrison, and R. G. Parr, Phys. Rev. A **50**, 2138 (1994).

[223] A. Becke, J. Chem. Phys. **104**, 1040 (1996).

[224] A. Savin, F. Colonna, and J.-M. Teuler, in *Electronic Density Functional Theory: Recent Progress and New Directions*, eds. J.F. Dobson, G. Vignale, and M.P. Das (Plenum, NY, 1997).

[225] E.K.U. Gross and S. Kurth in *Relativistic and Electron Correlation Effects in Molecules and Solids* ed. G.L. Malli (Nato ASI Series, Plenum, 1993).

Curriculum Vita

Takeyce Kamara Whittingham

EDUCATION

1998 B.A. in Chemistry, Rutgers University, New Brunswick, NJ (May 1998)

2004 Ph.D. in Chemistry, Rutgers University, New Brunswick, NJ

Employment

1998-2000	Fellow, Rutgers University
2000-2001	Teaching Assistant, Rutgers University Department of Chemistry
2002-2003	Fellow, Rutgers University
Fall 2003	Teaching Assistant, Rutgers University Department of Chemistry
Spring 2004	Fellow, Rutgers University

PUBLICATIONS

Synthesis and crystal structure analysis of selenostannates $[M(en)_3]_2Sn_2Se_6$*, M = Mn, Zn*,
T.K. Whittingham, Z. Chen, J. Li, and D.M. Prosperio, Bull. N.J. Acad. Sci. **42**, 11 (1998).

Oxidative addition of dihydrogen to $M(PH_3)_2Cl$*, M = Rh and Ir: A computational study using DFT and MO methods*,
M. Czerw, T.K. Whittingham, and K. Krogh-Jespersen in *Computational Organometallic Chemistry*, ed. T.R. Cundari,
(Marcel Dekker, Inc., New York, 2001).

Scaling the spin densities separately in density functional theory,
R.J. Magyar, T.K. Whittingham, and K. Burke, Phys Rev A **66**, 022105 (2002).

Correlation energies in the high density limit,
T.K. Whittingham and K. Burke, in preparation.